



HAL
open science

Strong competition between Θ_{II} -loop-current order and d -wave charge order along the diagonal direction in a two-dimensional hot spot model

Vanuildo S. de Carvalho, Thomas Kloss, Xavier Montiel, Hermann Freire,
Catherine Pépin

► To cite this version:

Vanuildo S. de Carvalho, Thomas Kloss, Xavier Montiel, Hermann Freire, Catherine Pépin. Strong competition between Θ_{II} -loop-current order and d -wave charge order along the diagonal direction in a two-dimensional hot spot model. *Physical Review B: Condensed Matter and Materials Physics* (1998-2015), 2015, 92 (7), pp.075123. 10.1103/PhysRevB.92.075123 . cea-01339333v1

HAL Id: cea-01339333

<https://cea.hal.science/cea-01339333v1>

Submitted on 29 Jun 2016 (v1), last revised 18 Oct 2022 (v2)

HAL is a multi-disciplinary open access archive for the deposit and dissemination of scientific research documents, whether they are published or not. The documents may come from teaching and research institutions in France or abroad, or from public or private research centers.

L'archive ouverte pluridisciplinaire **HAL**, est destinée au dépôt et à la diffusion de documents scientifiques de niveau recherche, publiés ou non, émanant des établissements d'enseignement et de recherche français ou étrangers, des laboratoires publics ou privés.

Strong competition between Θ_{II} -loop-current order and d -wave charge order along the diagonal direction in a two-dimensional hot spot model

Vanuildo S. de Carvalho^{1,2}, Thomas Kloss², Xavier Montiel², Hermann Freire^{1,*} and Catherine Pépin²

¹*Instituto de Física, Universidade Federal de Goiás, 74.001-970, Goiânia-GO, Brazil, and*

²*IPhT, L'Orme des Merisiers, CEA-Saclay, 91191 Gif-sur-Yvette, France*

(Dated: August 10, 2015)

We study the fate of the so-called Θ_{II} -loop-current order that breaks both time-reversal and parity symmetries in a two-dimensional hot spot model with antiferromagnetically mediated interactions, using Fermi surfaces relevant to the phenomenology of the cuprate superconductors. We start from a three-band Emery model describing the hopping of holes in the CuO_2 plane that includes two hopping parameters t_{pp} and t_{pd} , local on-site Coulomb interactions U_d and U_p and nearest-neighbor V_{pd} couplings between the fermions in the copper [$\text{Cu}(3d_{x^2-y^2})$] and oxygen [$\text{O}(2p_x)$ and $\text{O}(2p_y)$] orbitals. By focusing on the lowest-energy band, we proceed to decouple the local interaction U_d of the Cu orbital in the spin channel using a Hubbard-Stratonovich transformation to arrive at the interacting part of the so-called spin-fermion model. We also decouple the nearest-neighbor interaction V_{pd} to introduce the order parameter of the Θ_{II} -loop-current order. In this way, we are able to construct a consistent mean-field theory that describes the strong competition between the composite order parameter made of a quadrupole-density-wave and d -wave pairing fluctuations proposed in Efetov *et al.* [Nat. Phys. **9**, 442 (2013)] with the Θ_{II} -loop-current order parameter that is argued to be relevant for explaining important aspects of the physics of the pseudogap phase displayed in the underdoped cuprates.

PACS numbers: 74.20.Mn, 74.20.-z, 71.10.Hf

I. INTRODUCTION

The physics of the pseudogap phase of cuprate superconductors remains one of the most enduring open problems of condensed matter physics. There are recent pervasive hints that the pseudogap phase in most underdoped cuprate superconductors might involve one or more symmetry-breaking “hidden” orders, whose precise microscopic mechanisms are still elusive to this date. State-of-the-art experiments such as nuclear magnetic resonance^{1,2}, pulsed-echo ultrasound experiments³, x-ray scattering⁴⁻⁶ and scanning tunneling microscopy^{7,8} performed in non-Lanthanum-based materials established the emergence of a dome-shaped short-range incommensurate d -wave^{9,10} charge-density-wave (CDW) at low hole doping with a modulation described by the wavevectors $\mathbf{Q}_x = (Q_0, 0)$ and $\mathbf{Q}_y = (0, Q_0)$ oriented along the principal axes of the CuO_2 unit cell (with $Q_0 \simeq 0.255$ in reciprocal lattice units^{11,12}). Quite surprisingly, the peak of this short-range charge order dome occurs approximately at the universal hole doping $x \simeq 0.12$ for several compounds¹³, despite their differences in material-specific properties. This could suggest that simple, low-energy effective models may potentially capture the essence of the physics of these materials¹⁴⁻¹⁷. We will follow this point of view in the present work. Moreover, by applying pressure on these systems, the charge order can be completely suppressed, while the pseudogap phase remains unaffected¹³. This clearly indicates that such a CDW order emerges on top of an already-formed pseudogap phase, instead of being its driving force. On the other hand, at very high magnetic fields, the d -wave superconducting phase displayed by these materials is destroyed

and the short-range CDW turns into a long-range order. In this context, it plays a central role in reconstructing the Fermi surface of these compounds into pockets, as is evidenced in quantum oscillation experiments^{18,19}.

In addition to these salient features taking place within the pseudogap phase, another form of “hidden” order representing potentially one of the driving forces of quantum criticality in these systems (that may even coexist with CDW order and d -wave superconductivity at lower temperature scales $T < T^*$) is suggested by a different set of equally groundbreaking experiments: spin-polarized neutron scattering^{20,21} and Kerr-rotation experiments^{22,23} indicate spontaneous breaking of both time-reversal and parity symmetries in this phase at temperatures that are reasonably close to T^* over a wide doping range. This phase transition has thus been referred to as the Kerr transition in the literature. This transition was given a theoretical framework in the proposal by Varma²⁴ (see also an interesting, alternative proposal put forward in Ref.²⁵) that orbital loop current order – we shall specialize in the present work to the so-called Θ_{II} -phase – may account for the observed properties in these materials, since it naturally preserves the translational symmetry of the lattice and, additionally, it leads to the breaking of the correct discrete symmetries consistent with spin polarized neutron scattering experiments²⁶. This theoretical description requires starting from at least a three-band model, in which one includes besides the usually considered copper $d_{x^2-y^2}$ -orbital, also the oxygen p_x and p_y -orbitals of the CuO_2 unit cell. Such a minimal model turns out to be essential to describe intra-unit-cell loop currents involving charge transfer between oxygen orbitals that appear in the afore-

mentioned Θ_{II} -phase. This theoretical proposal is physically appealing but it has one potential disagreement with experiments: it is hard to obtain the result that the underlying Fermi surface gaps out at all, since the phase transition does not break translational symmetry near the hot spots (i.e. the points in momentum space where the Fermi surface intersects the antiferromagnetic Brillouin zone boundary). Moreover, it is important to mention that recently a quantum critical point (QCP) was revealed in the cuprates at a hole-doping $x_{crit} \simeq 0.18$ via an analysis of the quasiparticle mass enhancement using quantum oscillation experiments²⁷. Interestingly, this critical point may represent approximately the termination of the Kerr transition line, the charge-order-dome and an as-yet-unidentified third phase competing with the previous two orders at a doping level reasonably close to optimal doping.

On the theoretical front, the hot spot model emerges as an interesting, minimal low-energy effective model that captures qualitative aspects of the physics of the high- T_c cuprates from a weak-to-moderate coupling perspective. In this respect, an important work by Metlitski and Sachdev¹⁵ consisted in the elegant demonstration that, if the energy dispersion of this model is linearized, an exact emergent $SU(2)$ pseudospin symmetry relating a d -wave singlet superconducting (SSC) order to a d -wave quadrupole-density-wave (QDW) order at wavevectors along the Brillouin zone diagonal ($\pm Q_0, \pm Q_0$) is verified at the spin-density-wave (SDW) quantum critical point. This degeneracy between these two orders effectively produces a composite order parameter (denoted by QDW/SSC) with both bond order and preformed pairs at high temperatures as shown by Efetov *et al.*¹⁶ and the properties of this state have been explored in connection with the physics of the cuprates using different approaches in many works^{28–37}. In addition to this fact, another emergent $SU(2)$ degeneracy relating two additional orders – a superconducting order with a finite Cooper-pair center of mass momentum (the so-called pair-density-wave (PDW)^{38–40}) and a d -wave CDW at the experimentally observed wavevectors \mathbf{Q}_x and \mathbf{Q}_y – has also been recently verified in the model in the work by Pépin *et al.*⁴¹ and explored further by Wang *et al.*⁴². This additional degeneracy generates another composite order parameter (denoted by PDW/CDW) with similar energy scales that also competes with the QDW/SSC order^{41–43}.

In the present work, we will consider the relevant scenario in which yet another order parameter (the Θ_{II} -loop current order) competes with the QDW/SSC order in an effective hot spot model. The purpose of this study is to demonstrate the possibility that, due to this competition, QSW/SSC is strongly affected by the Θ_{II} -order parameter that breaks both time-reversal and parity symmetries, but instead preserves their product. This opens an interesting avenue for future research and could be an explanation as to why the charge-order signal in the cuprates is always observed along the axial vectors (i.e. \mathbf{Q}_x and \mathbf{Q}_y) and never along the diagonal direction. In

order to perform this investigation, we will construct a novel mean-field theory by including both Θ_{II} -loop current order and the QDW/SSC composite order parameter in such an effective model. As will become clear shortly, we will confirm in this analysis the strong competition between Θ_{II} -loop current order and the QDW/SSC entangled order, with one order parameter being clearly always detrimental to the other. Then we proceed to discuss the physical implications of this strong competition for the physics of the underdoped cuprates, in light of the recent experiments performed in these materials.

Technically speaking, we will introduce a three-band model (Emery model) describing hopping of holes in the CuO_2 plane which includes two hopping parameters t_{pp} and t_{pd} , on-site U_d and U_p local interactions and nearest-neighbor V_{pd} couplings between the fermions in the copper ($d_{x^2-y^2}$) and oxygen (p_x and p_y) orbitals. By focussing on the lowest-energy band, we will decouple the local interaction U_d of the Cu orbital in the spin channel using a conventional Hubbard-Stratonovich transformation to arrive at the interacting part of the so-called spin-fermion model. Then, we will follow closely the methodology explained in full detail in the paper by Efetov *et al.*¹⁶ to define the composite order parameter associated with the QDW/SSC fluctuations. In addition to this, we will also decouple the nearest-neighbor interaction V_{pd} of the model to introduce the order parameter associated with the Θ_{II} -loop-current order. Lastly, we will proceed to derive analytically and then solve numerically the resulting mean-field equations, which describes the competition between these two order parameters.

This paper is organized as follows. In Section II, we define the three-band model that we will be interested in and we show how to decouple the interactions to obtain the resulting mean-field equations describing the competition between the two orders. Since the interactions that promote QDW/SSC and Θ_{II} -loop current order turn out to be different, this decoupling is unambiguous. In Section III, we solve numerically the self-consistent mean-field equations and then we discuss our main results. Finally, Section IV is devoted to our conclusions.

II. THE THREE-BAND MODEL

We start this section by writing down both the non-interacting and interacting Hamiltonians of the so-called three-band (Emery) model following Refs.^{44–47} in order to describe the underdoped cuprates as follows

$$\begin{aligned} \mathcal{H}_0 = & -t_{pd} \sum_{i,\sigma} \sum_{\nu} (\hat{d}_{i,\sigma}^{\dagger} \hat{p}_{i+\hat{\nu}/2,\sigma} + H.c.) \\ & - t_{pp} \sum_{i,\sigma} \sum_{\langle \nu, \nu' \rangle} (\hat{p}_{i+\hat{\nu}/2,\sigma}^{\dagger} \hat{p}_{i+\hat{\nu}'/2,\sigma} + H.c.) \\ & + (\varepsilon_d - \mu) \sum_{i,\sigma} \hat{n}_{i,\sigma}^d + \frac{1}{2} (\varepsilon_p - \mu) \sum_{i,\sigma} \sum_{\nu} \hat{n}_{i+\hat{\nu}/2,\sigma}^p, \quad (1) \end{aligned}$$

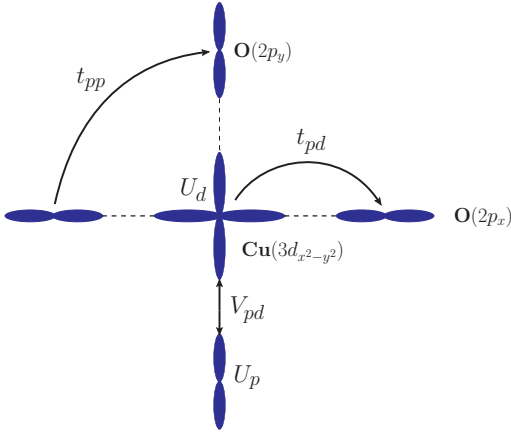


FIG. 1: (Color online) Orbital structure and the interactions of the three-band model in the CuO_2 unit cell.

$$\begin{aligned} \mathcal{H}_{int} = & U_d \sum_i \hat{n}_{i,\uparrow}^d \hat{n}_{i,\downarrow}^d + \frac{U_p}{2} \sum_{i,\nu} \hat{n}_{i+\hat{\nu}/2,\uparrow}^p \hat{n}_{i+\hat{\nu}/2,\downarrow}^p \\ & + V_{pd} \sum_{i,\nu} \sum_{\sigma,\sigma'} \hat{n}_{i,\sigma}^d \hat{n}_{i+\hat{\nu}/2,\sigma'}^p. \end{aligned} \quad (2)$$

This model Hamiltonian describes the fermionic motion on the copper [$\text{Cu}(3d_{x^2-y^2})$] and oxygen [$\text{O}(2p_x)$ and $\text{O}(2p_y)$] orbitals that are located in the CuO_2 unit cell (see Fig. 1). The quantities $\hat{d}_{i,\sigma}^\dagger$, $\hat{d}_{i,\sigma}$, $\hat{p}_{i+\hat{\nu}/2,\sigma}^\dagger$ and $\hat{p}_{i+\hat{\nu}/2,\sigma}$ are, respectively, the creation and annihilation operators of fermions situated on the site i with spin σ of the Cu orbital and the the creation and annihilation operators of fermions on the site $i + \hat{\nu}/2$ ($\nu = x, y$) with spin σ of the O orbitals. Besides, $\hat{n}_{i,\sigma}^d$ and $\hat{n}_{i+\hat{\nu}/2,\sigma}^p$ correspond, respectively, to the fermionic number operators for particles located on the Cu and O orbitals. The model also takes into account pair hopping (t_{pd} and t_{pp}), on-site (U_d and U_p) and nearest-neighbor (V_{pd}) interactions involving the fermions on the Cu and O orbitals. The parameters ε_d and ε_p are, respectively, the Cu and O orbital energies and μ is the chemical potential which controls the electronic density in the system.

Following Abanov and Chubukov¹⁴, we first decouple the U_d part of the interacting Hamiltonian in the spin channel using a conventional Hubbard-Stratonovich transformation. The resulting action becomes

$$\begin{aligned} \mathcal{S}_{int}^{(1)}[d, \vec{\phi}] &= \lambda \int d\tau \sum_i d_{i,\sigma}^\dagger \vec{\phi}_i \cdot \vec{\sigma}_{\sigma,\sigma'} d_{i,\sigma'} e^{i\mathbf{Q}\cdot\mathbf{r}_i} \\ &+ \frac{1}{2} \int d\tau d^2\mathbf{r} \left[\frac{1}{v_s^2} (\partial_\tau \vec{\phi})^2 + (\nabla \vec{\phi})^2 + m_a \vec{\phi}^2 + \frac{g}{2} ((\vec{\phi})^2)^2 \right], \end{aligned} \quad (3)$$

where the bosonic field $\vec{\phi}_i = (\phi_i^x, \phi_i^y, \phi_i^z)$ is the spin-density wave (SDW) order parameter at the antiferromagnetic wave vector $\mathbf{Q} = (\pi, \pi)$, v_s is the spin-wave

velocity, and m_a is the spin-wave bosonic mass which vanishes at the quantum critical point (QCP) of the theory. The σ^a ($a = x, y, z$) are the usual Pauli matrices. Notice that in Eq. (3) we have partially integrated out the high-energy fermions in order to derive an effective theory $\mathcal{S}_{int}^{(1)}[d, \vec{\phi}]$ that corresponds to the so-called spin-fermion model describing the coupling between the itinerant low-energy fermionic excitations and the antiferromagnetic SDW fluctuations. Another possibility in order to investigate the Emery model is to start from a more localized picture by mapping the model defined in Eqs. (1) and (2) onto an effective three-band $t - J$ model⁴⁸. We, however, will not follow this latter route in the present work. For this reason, we would like to state clearly from the outset that our starting point here will be a more itinerant picture.

Now we turn our attention to the V_{pd} interaction term in Eq. (2). This can be rewritten as

$$V_{pd} \sum_{i,\nu} \sum_{\sigma,\sigma'} \hat{n}_{i,\sigma}^d \hat{n}_{i+\hat{\nu}/2,\sigma'}^p = -V_{pd} \sum_{i,j} \sum_{\sigma,\sigma'} \mathcal{A}_{i,\sigma}^\dagger(j) \mathcal{A}_{i,\sigma'}(j), \quad (4)$$

with the field operators on the right-hand-side of the above equality being

$$\begin{aligned} \mathcal{A}_{i,\sigma}^\dagger(1,2) &= \frac{1}{2} [(d_{i,\sigma}^\dagger \hat{p}_{i+\hat{x}/2,\sigma} + d_{i,\sigma}^\dagger \hat{p}_{i-\hat{x}/2,\sigma}) \\ &\pm (d_{i,\sigma}^\dagger \hat{p}_{i+\hat{y}/2,\sigma} + d_{i,\sigma}^\dagger \hat{p}_{i-\hat{y}/2,\sigma})], \end{aligned} \quad (5)$$

$$\begin{aligned} \mathcal{A}_{i,\sigma}^\dagger(3,4) &= \frac{i}{2} [(d_{i,\sigma}^\dagger \hat{p}_{i+\hat{x}/2,\sigma} - d_{i,\sigma}^\dagger \hat{p}_{i-\hat{x}/2,\sigma}) \\ &\pm (d_{i,\sigma}^\dagger \hat{p}_{i+\hat{y}/2,\sigma} - d_{i,\sigma}^\dagger \hat{p}_{i-\hat{y}/2,\sigma})]. \end{aligned} \quad (6)$$

As first shown by Varma²⁴, only the order parameters associated with $\mathcal{A}_{i,\sigma}^{(2)}$, $\mathcal{A}_{i,\sigma}^{(3)}$, and $\mathcal{A}_{i,\sigma}^{(4)}$ lead to states with the presence of stationary-loop currents on the CuO_2 plane and, of course, to time-reversal symmetry breaking. The loop-current order with order parameter defined in terms of $\mathcal{A}_{i,\sigma}^{(2)}$ is conventionally called the Θ_I -loop current phase,

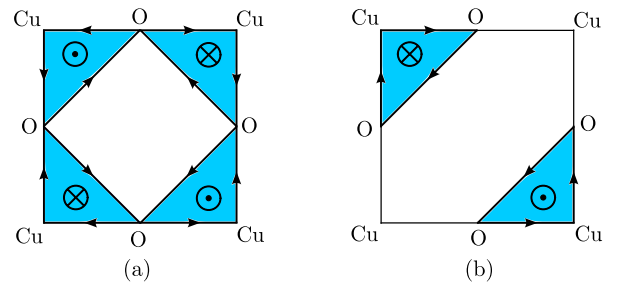


FIG. 2: (Color online) Loop current pattern in the CuO_2 unit cell for the Θ_I - and Θ_{II} -loop current phases [panels (a) and (b), respectively] proposed by Varma to explain the physical properties of the pseudogap state in high- T_c cuprate superconductors. The symbols (\odot) and (\otimes) represent the orientation of the local magnetic moments generated by the loop currents.

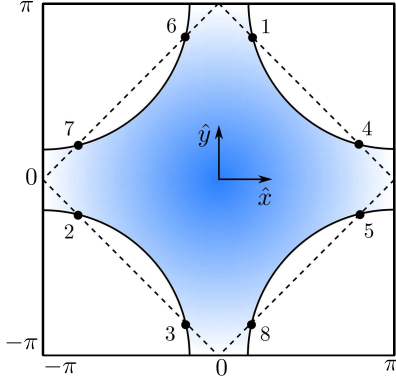


FIG. 3: (Color online) Representation of the Brillouin zone with the underlying noninteracting Fermi surface (that encloses the blue area) which characterizes the underdoped cuprate superconductors. The small black circles denote the so-called hot spots which are defined as the intersection of the Fermi surface with the antiferromagnetic zone boundary. For instance, the hot spot labeled as 1 has a wavevector $\mathbf{k}_1 = (K_-, K_+)$ in momentum space with the constraint $K_- + K_+ = \pi$. The wavevectors of all the other hot spots in the Brillouin zone are obtained by simple symmetry operations.

while the loop-current order with order parameter given in terms of $\mathcal{A}_{i,\sigma}^{(3)}$, and $\mathcal{A}_{i,\sigma}^{(4)}$ are known as the Θ_{II} -loop current phase (see Fig. 2). In view of the interpretation of some experiments on the pseudogap phase of the cuprate superconductors as an evidence in favor of the Θ_{II} -loop current phase^{20,26}, we will analyze henceforth only this type of order. In this way, the decoupling of the interacting term in Eq. (4) using a Hubbard-Stratonovich transformation yields the following expression

$$\begin{aligned} & \exp \left\{ V_{pd} \int d\tau \sum_i \sum_{\sigma, \sigma'} \mathcal{A}_{i,\sigma}^{\dagger(3)} \mathcal{A}_{i,\sigma'}^{(3)} \right\} \\ &= \int \mathcal{D}[R_{II}, \Theta_{II}] \exp \left\{ \int d\tau \sum_{i,\sigma} \left[-\frac{R_{II}^2}{2V_{pd}} + R_{II} e^{i\Theta_{II}} \mathcal{A}_{i,\sigma}^{\dagger(3)} \right. \right. \\ & \left. \left. + R_{II} e^{-i\Theta_{II}} \mathcal{A}_{i,\sigma}^{(3)} \right] \right\}, \end{aligned} \quad (7)$$

where $R_{II} e^{i\Theta_{II}} = V_{pd} \sum_{\sigma} \langle \mathcal{A}_{i,\sigma}^{(3)} \rangle$ is a complex order parameter. The mean-field value of the phase Θ_{II} was determined in Ref.²⁴ as being equal to $\pm\pi/2$. In what follows, we will choose for simplicity the positive value of Θ_{II} , since it has been shown in Ref.²⁴ that this choice minimizes the energy for the present case.

At this point, we would like to point out that we will consider only the lowest energy band of the noninteracting Hamiltonian defined in Eq. (1). For physically motivated choices of the parameters in the present model, the low-energy band will naturally give rise to a Fermi surface shown in Fig. 3. The most singular contribution in this effective model will arise from the points at the Fermi surface (the so-called hot spots) that represents the intersection of this surface with the antiferromagnetic zone boundary. Therefore, we will restrict the analysis of the present model to the vicinity of these important hot spot points in the considerations that follow. With this in mind and to set up our notation, we now define the following 16-component fermionic spinors

$$d = \begin{pmatrix} \begin{pmatrix} d_1 \\ d_2 \\ d_3 \\ d_4 \end{pmatrix}_{\Sigma} \\ \begin{pmatrix} d_5 \\ d_6 \\ d_7 \\ d_8 \end{pmatrix}_{\Sigma} \end{pmatrix}_{\Lambda} \quad , \quad p_{x(y)} = \begin{pmatrix} \begin{pmatrix} p_{x(y)1} \\ p_{x(y)2} \\ p_{x(y)3} \\ p_{x(y)4} \end{pmatrix}_{\Sigma} \\ \begin{pmatrix} p_{x(y)5} \\ p_{x(y)6} \\ p_{x(y)7} \\ p_{x(y)8} \end{pmatrix}_{\Sigma} \end{pmatrix}_{\Lambda} \quad , \quad (8)$$

where $d_i = \begin{pmatrix} d_{i,\uparrow} \\ d_{i,\downarrow} \end{pmatrix}_{\sigma}$ and $p_{x(y)i} = \begin{pmatrix} p_{x(y)i,\uparrow} \\ p_{x(y)i,\downarrow} \end{pmatrix}_{\sigma}$ are also spinors in the spin space σ . The symbols Σ , Λ , and L represent independent pseudospin spaces that are generated by the Pauli matrices¹⁶. By making use of the results in Eq. (1), (3), (7), and (8) and linearizing the excitation spectrum of three-band model around the hot spots, we obtain that the total action of the system yields

$$\begin{aligned} \mathcal{S}[p_x, p_y, d, \vec{\phi}; n_p, R_{II}] &= \mathcal{S}_0[p_x, p_y, d] + \mathcal{S}_{int}^{(1)}[d, \vec{\phi}] + \mathcal{S}_{int}^{(2)}[p_x, p_y, d; n_p, R_{II}] \\ &= \int (p_x^\dagger(X), p_y^\dagger(X), d^\dagger(X)) \begin{pmatrix} \partial_\tau + \xi_p & \hat{\Gamma}_1 + \hat{\Gamma}_2(-i\nabla) & \hat{\Gamma}_{1x} - \hat{\Gamma}_{2x}i\partial_x \\ \hat{\Gamma}_1 + \hat{\Gamma}_2(-i\nabla) & \partial_\tau + \xi_p & \Gamma_{1y} - \Gamma_{2y}i\partial_y \\ \hat{\Gamma}_{1x} - \hat{\Gamma}_{2x}i\partial_x & \hat{\Gamma}_{1y} - \hat{\Gamma}_{2y}i\partial_y & \partial_\tau + \xi_d \end{pmatrix} \begin{pmatrix} p_x(X) \\ p_y(X) \\ d(X) \end{pmatrix} dX \\ &+ \frac{1}{2} \int \left[\frac{1}{v_s^2} (\partial_\tau \vec{\phi})^2 + (\nabla \vec{\phi})^2 + m_a \vec{\phi}^2 + \frac{g}{2} (\vec{\phi}^2)^2 \right] dX + \lambda \int [d^\dagger(X) \Sigma_1 \vec{\phi}(X) \vec{\sigma} d(X)] dX \\ &+ \int \left(\frac{R_{II}^2}{V_{pd}} - \frac{n_p^2}{8} U_p \right) dX, \end{aligned} \quad (9)$$

where $\xi_p \equiv \varepsilon_p + \frac{n_p}{4}U_p - \mu$, $\xi_d \equiv \varepsilon_d - \mu$, and both time and space coordinates have been collected in terms of the variable $X = (\tau, \mathbf{r})$. The matrices $\hat{\Gamma}_1, \hat{\Gamma}_2, \hat{\Gamma}_{1x(y)}$, and $\hat{\Gamma}_{2x(y)}$ appearing in Eq. (9) are diagonal in the $\Sigma \otimes \Lambda \otimes L$ pseudospin space and depend on all the parameters of the three-band model and also on the order parameter R_{II} for the Θ_{II} -loop current phase (see the Appendix A to check their definition). Here we follow Ref.¹⁶ and introduce the 32-component fermionic spinors in the particle-hole space τ as

$$\Psi = \frac{1}{\sqrt{2}} \begin{pmatrix} d^* \\ i\sigma_2 d \end{pmatrix}_\tau, \Psi^\dagger = \frac{1}{\sqrt{2}} (-d^\dagger, -d^\dagger i\sigma_2)_\tau, \quad (10)$$

$$P_x = \frac{1}{\sqrt{2}} \begin{pmatrix} P_x^* \\ i\sigma_2 P_x \end{pmatrix}_\tau, P_x^\dagger = \frac{1}{\sqrt{2}} (-P_x^\dagger, -P_x^\dagger i\sigma_2)_\tau, \quad (11)$$

$$P_y = \frac{1}{\sqrt{2}} \begin{pmatrix} P_y^* \\ i\sigma_2 P_y \end{pmatrix}_\tau, P_y^\dagger = \frac{1}{\sqrt{2}} (-P_y^\dagger, -P_y^\dagger i\sigma_2)_\tau. \quad (12)$$

In addition to the fermionic fields defined above, we also introduce the charge-conjugated vectors as

$$\bar{\Psi} = \Psi^\dagger \tau_3, \quad \bar{P}_x = P_x^\dagger \tau_3, \quad \bar{P}_y = P_y^\dagger \tau_3, \quad (13)$$

where τ_3 is the usual Pauli matrix defined in the τ space. Hence by making use of these last definitions, the action in Eq. (9) can be naturally rewritten as

$$\begin{aligned} & \mathcal{S}[P_x, P_y, \Psi, \vec{\phi}; n_p, R_{II}] \\ &= \int (\bar{P}_x(X), \bar{P}_y(X), \bar{\Psi}(X)) \begin{pmatrix} -\partial_\tau + \xi_p \tau_3 & \hat{\Gamma}_1 \tau_3 - \hat{\Gamma}_2 (-i\nabla) & \hat{\Gamma}_{1x} \tau_3 + \hat{\Gamma}_{2x} i\partial_x \\ \hat{\Gamma}_1 \tau_3 - \hat{\Gamma}_2 (-i\nabla) & -\partial_\tau + \xi_p \tau_3 & \hat{\Gamma}_{1y} \tau_3 + \hat{\Gamma}_{2y} i\partial_y \\ \hat{\Gamma}_{1x}^\dagger \tau_3 + \hat{\Gamma}_{2x}^\dagger i\partial_x & \hat{\Gamma}_{1y}^\dagger \tau_3 + \hat{\Gamma}_{2y}^\dagger i\partial_y & -\partial_\tau + \xi_d \tau_3 \end{pmatrix} \begin{pmatrix} P_x(X) \\ P_y(X) \\ \Psi(X) \end{pmatrix} dX \\ &+ \lambda \int [\bar{\Psi}(X) \Sigma_1 \vec{\phi}(X) \vec{\sigma}^t \Psi(X)] dX + \frac{1}{2} \int \left[\frac{1}{v_s^2} (\partial_\tau \vec{\phi})^2 + (\nabla \vec{\phi})^2 + m_a \vec{\phi}^2 + \frac{g}{2} (\vec{\phi}^2)^2 \right] dX \\ &+ \int \left(\frac{R_{II}^2}{V_{pd}} - \frac{n_p^2}{8} U_p \right) dX. \end{aligned} \quad (14)$$

In order to derive the thermodynamical properties of the present model, we should first integrate out the bosonic field in the functional integral

$$\begin{aligned} \mathcal{Z} &= \int \exp\left\{-\mathcal{S}[P_x, P_y, \Psi, \vec{\phi}; n_p, R_{II}]\right\} \mathcal{D}[P_x, P_y, \Psi, \vec{\phi}] \\ &= \int \exp\left\{-\mathcal{S}[P_x, P_y, \Psi; n_p, R_{II}]\right\} \mathcal{D}[P_x, P_y, \Psi]. \end{aligned} \quad (15)$$

However, before proceeding with that, we will neglect from now on the spin-density-wave interaction g in the present model, since this coupling effectively renormalizes to zero under the RG flow in the low-energy limit¹⁶. As a result, the partition function of the three-band model may be computed in closed form giving rise to the low-energy effective action

$$\begin{aligned} & \mathcal{S}[P_x, P_y, \Psi; n_p, R_{II}] \\ &= \int (\bar{P}_x(X), \bar{P}_y(X), \bar{\Psi}(X)) \begin{pmatrix} -\partial_\tau + \xi_p \tau_3 & \hat{\Gamma}_1 \tau_3 - \hat{\Gamma}_2 (-i\nabla) & \hat{\Gamma}_{1x} \tau_3 + \hat{\Gamma}_{2x} i\partial_x \\ \hat{\Gamma}_1 \tau_3 - \hat{\Gamma}_2 (-i\nabla) & -\partial_\tau + \xi_p \tau_3 & \hat{\Gamma}_{1y} \tau_3 + \hat{\Gamma}_{2y} i\partial_y \\ \hat{\Gamma}_{1x}^\dagger \tau_3 + \hat{\Gamma}_{2x}^\dagger i\partial_x & \hat{\Gamma}_{1y}^\dagger \tau_3 + \hat{\Gamma}_{2y}^\dagger i\partial_y & -\partial_\tau + \xi_d \tau_3 \end{pmatrix} \begin{pmatrix} P_x(X) \\ P_y(X) \\ \Psi(X) \end{pmatrix} dX \\ &- \frac{\lambda^2}{2} \int [\bar{\Psi}(X) \Sigma_1 \vec{\sigma}^t \Psi(X)] D(X - X') [\bar{\Psi}(X') \Sigma_1 \vec{\sigma}^t \Psi(X')] dX dX' + \int \left(\frac{R_{II}^2}{V_{pd}} - \frac{n_p^2}{8} U_p \right) dX. \end{aligned} \quad (16)$$

Here the function $D(X - X')$ that appears as a potential function in the fermionic quartic interaction is the bare bosonic propagator. Its Fourier transform is given by $D(\omega, \mathbf{k}) = (\omega^2/v_s^2 + |\mathbf{k}|^2 + m_a)^{-1}$ with m_a standing for the spin-wave boson mass that vanishes at the QCP, v_s

is the spin-wave velocity and ω denotes the Matsubara bosonic frequency.

Next, we decouple the fermionic quartic term of the action in Eq. (16) by using a composite order parameter $M(X, X')$ for both the quadrupole density wave (QDW)

and the d -wave singlet superconducting (SSC) orders, as was described in full detail in Ref.¹⁶. This is achieved by considering the renormalization of bosonic propagator $D(\omega, \mathbf{k})$ by the fermions at the hot spots which leads to the appearance of the effective spin-wave propagator

$D_{eff}(\omega, \mathbf{k}) = (\gamma|\omega| + |\mathbf{k}|^2 + m_a)^{-1}$, where γ is naturally the Landau damping term. As a consequence, the low-energy effective action that describes the present system may be represented as follows

$$\begin{aligned} & \mathcal{S}_{eff}[P_x, P_y, \Psi; n_p, R_{II}, M] \\ &= \int (\bar{P}_x(X), \bar{P}_y(X), \bar{\Psi}(X)) \begin{pmatrix} -\partial_\tau + \xi_p \tau_3 & \hat{\Gamma}_1 \tau_3 - \hat{\Gamma}_2(-i\nabla) & \hat{\Gamma}_{1x} \tau_3 + \hat{\Gamma}_{2x} i \partial_x \\ \hat{\Gamma}_1^\dagger \tau_3 - \hat{\Gamma}_2^\dagger(-i\nabla) & -\partial_\tau + \xi_p \tau_3 & \hat{\Gamma}_{1y} \tau_3 + \hat{\Gamma}_{2y} i \partial_y \\ \hat{\Gamma}_{1x}^\dagger \tau_3 + \hat{\Gamma}_{2x}^\dagger i \partial_x & \hat{\Gamma}_{1y}^\dagger \tau_3 + \hat{\Gamma}_{2y}^\dagger i \partial_y & -\partial_\tau + \xi_d \tau_3 \end{pmatrix} \begin{pmatrix} P_x(X) \\ P_y(X) \\ \Psi(X) \end{pmatrix} dX \\ &- i \int \bar{\Psi}(X) M(X, X') \Psi(X') dX dX' + \frac{1}{2} \int J^{-1}(X - X') \text{Tr}[M(X, X') \Sigma_1 M(X', X) \Sigma_1] dX dX' \\ &+ \int \left(\frac{R_{II}^2}{V_{pd}} - \frac{n_p^2}{8} U_p \right) dX, \end{aligned} \quad (17)$$

where we have written $J(X - X') = 3\lambda^2 D_{eff}(X - X')$ instead of the spin-wave propagator in order to simplify the notation. The order parameter $M(X, X')$ for the QDW/SSC composite order is given by

$$M(X, X') = b(X, X') \Sigma_3 \begin{pmatrix} 0 & \hat{u}_\tau \\ -\hat{u}_\tau^\dagger & 0 \end{pmatrix}_\Lambda, \quad (18)$$

$$\text{with } \hat{u}_\tau = \begin{pmatrix} \Delta_- & \Delta_+ \\ -\Delta_+^* & \Delta_-^* \end{pmatrix}_\tau. \quad (19)$$

Here Δ_+ and Δ_- are, respectively, the d -wave singlet superconducting (SSC) and quadrupole density wave (QDW) components of the order parameter defined above. We also point out that the matrices \hat{u}_τ belong to the $SU(2)$ group¹⁶ which lead to the constraint $|\Delta_+|^2 + |\Delta_-|^2 = 1$ involving both the SSC and QDW sectors. Although we have constructed an effective spin-fermion model for the CuO_2 unit cell by considering only the Cu atoms, we point out that the QDW/SSC order parameter in Eq. (18) does not lead to a charge modulation located on the Cu orbitals. In fact, it can be shown^{16,28,29} that this composite order parameter generates a charge modulation with a checkerboard pattern residing on the oxygen O sites, which is described by incommensurate wavevectors with respect to the lattice.

The effective action in Eq. (17) now has a quadratic form and the free energy of the system can be obtained as follows: First one has to integrate out the fermionic fields in the functional integral for the partition function and then apply the formulae $\text{Tr} \ln G^{-1} = \ln \det(G^{-1})$. Following this procedure, we determine that the free energy

in space-time coordinates evaluates to

$$\begin{aligned} & \frac{F[T, n_p, R_{II}, M]}{T} = - \int \text{Tr} \ln[G^{-1}(X, X')] dX dX' \\ &+ \frac{1}{2} \int J^{-1}(X - X') \text{Tr}[M(X, X') \Sigma_1 M(X', X) \Sigma_1] dX dX' \\ &+ \int \left(\frac{R_{II}^2}{V_{pd}} - \frac{n_p^2}{8} U_p \right) dX, \end{aligned} \quad (20)$$

where the matrix $G^{-1}(X, X')$ is the Fourier transform of $G^{-1}(i\varepsilon_n, \mathbf{k})$. This latter function is given by

$$\begin{pmatrix} -i\varepsilon_n + \xi_p \tau_3 & \hat{\Gamma}_1 \tau_3 - \hat{\Gamma}_2(\mathbf{k}) & \hat{\Gamma}_{1x} \tau_3 - \hat{\Gamma}_{2x} k_x \\ \hat{\Gamma}_1^\dagger \tau_3 - \hat{\Gamma}_2^\dagger(\mathbf{k}) & -i\varepsilon_n + \xi_p \tau_3 & \hat{\Gamma}_{1y} \tau_3 - \hat{\Gamma}_{2y} k_y \\ \hat{\Gamma}_{1x}^\dagger \tau_3 - \hat{\Gamma}_{2x}^\dagger k_x & \hat{\Gamma}_{1y}^\dagger \tau_3 - \hat{\Gamma}_{2y}^\dagger k_y & -i\varepsilon_n + \xi_d \tau_3 - iM(\varepsilon_n, \mathbf{k}) \end{pmatrix}. \quad (21)$$

The self-consistency equation for $b(X, X')$ is derived by minimizing the free energy $F[T, n_p, R_{II}, M]$ with respect to this order parameter. As a consequence, we obtain the following equation

$$\begin{aligned} & - \text{Tr} \left\{ \frac{1}{G^{-1}(X, X')} \frac{\partial G^{-1}(X, X')}{\partial b(X, X')} \right\} + J^{-1}(X - X') b(X, X') \\ & \times \text{Tr} \left\{ \Sigma_3 \begin{pmatrix} 0 & \hat{u}_\tau \\ -\hat{u}_\tau^\dagger & 0 \end{pmatrix}_\Lambda \Sigma_1 \Sigma_3 \begin{pmatrix} 0 & \hat{u}_\tau \\ -\hat{u}_\tau^\dagger & 0 \end{pmatrix}_\Lambda \Sigma_1 \right\} = 0. \end{aligned} \quad (22)$$

By performing the trace operation over the space $\Sigma \otimes \Lambda \otimes L \otimes \tau$ for the second term on the left-hand-side of the equation above, the order parameter $b(X, X')$ can be

simply expressed as

$$\begin{aligned}
b(X, X') &= \frac{1}{16} J(X - X') \text{Tr} \left\{ G(X, X') \frac{\partial G^{-1}(X, X')}{\partial b(X, X')} \right\} \\
&= \frac{1}{16} J(X - X') \text{Tr} \left\{ G(X, X') i \Pi_3 \Sigma_3 \begin{pmatrix} 0 & \hat{u}_\tau \\ -\hat{u}_\tau^\dagger & 0 \end{pmatrix}_\Lambda \right\}, \tag{23}
\end{aligned}$$

where Π_3 is a projector for the three-band-model space which is defined as

$$\Pi_3 = \begin{pmatrix} 0 & 0 & 0 \\ 0 & 0 & 0 \\ 0 & 0 & 1 \end{pmatrix}. \tag{24}$$

At this point, we will make use of the ansatz $b(X, X') = b(X - X')$ [and $G(X, X') = G(X - X')$] and Fourier transform Eq. (23) to momentum-frequency space. As a result, we get the expression

$$\begin{aligned}
b(\varepsilon_n, \mathbf{k}) &= \frac{T}{16} \sum_{\varepsilon'_n} \int J(\varepsilon_n - \varepsilon'_n, \mathbf{k} - \mathbf{k}') \text{Tr} \left\{ [G^{-1}(i\varepsilon'_n, \mathbf{k}')]^{-1} \right. \\
&\quad \left. \times \frac{\partial G^{-1}(i\varepsilon'_n, \mathbf{k}')}{\partial b(\varepsilon'_n, \mathbf{k}')} \right\} \frac{d\mathbf{k}}{(2\pi)^2}. \tag{25}
\end{aligned}$$

In order to express $b(\varepsilon_n, \mathbf{k})$ in a convenient form, we need to evaluate the trace that appears in the above equation. This problem can be circumvented by using the following identity

$$\begin{aligned}
&\text{Tr} \left\{ [G^{-1}(i\varepsilon'_n, \mathbf{k}')]^{-1} \frac{\partial G^{-1}(i\varepsilon'_n, \mathbf{k}')}{\partial b(\varepsilon'_n, \mathbf{k}')} \right\} \\
&= \frac{1}{\det[G^{-1}(i\varepsilon'_n, \mathbf{k}')] } \frac{\partial \det[G^{-1}(i\varepsilon'_n, \mathbf{k}')] }{\partial b(\varepsilon'_n, \mathbf{k}')} . \tag{26}
\end{aligned}$$

Then, by substituting Eq. (26) into Eq. (25), we finally arrive at the self-consistency equation

$$\begin{aligned}
b(\varepsilon_n, \mathbf{k}) &= \frac{3\lambda^2 T}{16} \sum_{\varepsilon'_n} \int \frac{D_{eff}(\varepsilon_n - \varepsilon'_n, \mathbf{k} - \mathbf{k}')}{\det[G^{-1}(i\varepsilon'_n, \mathbf{k}')] } \\
&\quad \times \frac{\partial \det[G^{-1}(i\varepsilon'_n, \mathbf{k}')] }{\partial b(\varepsilon'_n, \mathbf{k}')} \frac{d\mathbf{k}}{(2\pi)^2}, \tag{27}
\end{aligned}$$

where we have set $J(\varepsilon_n - \varepsilon'_n, \mathbf{k} - \mathbf{k}') = 3\lambda^2 D_{eff}(\varepsilon_n - \varepsilon'_n, \mathbf{k} - \mathbf{k}')$.

We now turn our attention to the evaluation of $\det[G^{-1}(i\varepsilon_n, \mathbf{k})]$. In order to do this, we will need to use the set of determinant formulas

$$\det \begin{pmatrix} \hat{A} & \hat{B} \\ \hat{C} & \hat{D} \end{pmatrix} = \det(\hat{A}) \det(\hat{D} - \hat{C} \hat{A}^{-1} \hat{B}), \tag{28}$$

$$\det(\hat{A} \otimes \hat{D}) = [\det(\hat{A})]^m [\det(\hat{D})]^n, \tag{29}$$

where \hat{A} and \hat{D} are, respectively, n - and m -square matrices and $\det(\hat{A})$ is different from zero. In this way, by

neglecting the SSC sector of the QDW/SSC order parameter ($\Delta_+ = 0$) and applying these reduction formulas to the matrix $G^{-1}(i\varepsilon_n, \mathbf{k})$, we obtain, after some algebraic manipulations, that $\det[G^{-1}(i\varepsilon_n, \mathbf{k})]$ evaluates formally to

$$\det[G^{-1}(i\varepsilon_n, \mathbf{k})] = \prod_{l=1}^2 \prod_{m=1}^2 \mathcal{D}_l^{(m)}(i\varepsilon_n, \mathbf{k}), \tag{30}$$

where $\mathcal{D}_l^{(m)}(i\varepsilon_n, \mathbf{k})$ are well-behaved functions of the three-band-model parameters, which are computed in detailed form in Appendices B and C. Thus, by inserting the result displayed in Eq. (30) into Eq. (27), the mean-field equation for $b(\varepsilon_n, \mathbf{k})$ in terms of $\mathcal{D}_l^{(m)}(i\varepsilon_n, \mathbf{k})$ finally reads

$$\begin{aligned}
b(\varepsilon_n, \mathbf{k}) &= \frac{3\lambda^2 T}{16} \sum_{l,m=1}^2 \sum_{\varepsilon'_n} \int \frac{D_{eff}(\varepsilon_n - \varepsilon'_n, \mathbf{k} - \mathbf{k}')}{\mathcal{D}_l^{(m)}(i\varepsilon'_n, \mathbf{k}')} \\
&\quad \times \frac{\partial \mathcal{D}_l^{(m)}(i\varepsilon'_n, \mathbf{k}')}{\partial b(\varepsilon'_n, \mathbf{k}')} \frac{d\mathbf{k}'}{(2\pi)^2}. \tag{31}
\end{aligned}$$

We note that, since we have set $\Delta_+ = 0$, the above self-consistency equation describes only the QDW sector of the fluctuations in the present system.

As a consequence of the result in Eq. (30), we determine after Fourier transforming the right-hand-side of Eq. (20) that the free energy of the present model has the following analytical form

$$\begin{aligned}
F[T, n_p, R_{II}, b] &= -T \sum_{l,m=1}^2 \sum_{\varepsilon_n} \int \ln[\mathcal{D}_l^{(m)}(i\varepsilon_n, \mathbf{k})] \frac{d\mathbf{k}}{(2\pi)^2} \\
&\quad + \frac{8T}{3\lambda^2} \sum_{\varepsilon_n} \int b(\varepsilon_n, \mathbf{k}) \frac{d\mathbf{k}}{(2\pi)^2} \left[T \sum_{\varepsilon'_n} \int b(\varepsilon'_n, \mathbf{k}') \right. \\
&\quad \left. \times D_{eff}^{-1}(\varepsilon_n - \varepsilon'_n, \mathbf{k} - \mathbf{k}') \frac{d\mathbf{k}'}{(2\pi)^2} \right] + \frac{R_{II}^2}{V_{pd}} - \frac{n_p^2}{8} U_p, \tag{32}
\end{aligned}$$

where we have set the volume of the system to unity. In order to self-consistently determine the mean-field order parameter R_{II} , we need also minimize the free energy with respect to it. In this way, the self-consistency equation for R_{II} in turn reads

$$R_{II} = \frac{V_{pd} T}{2} \sum_{l,m=1}^2 \sum_{\varepsilon_n} \int \frac{1}{\mathcal{D}_l^{(m)}(i\varepsilon_n, \mathbf{k})} \frac{\partial \mathcal{D}_l^{(m)}(i\varepsilon_n, \mathbf{k})}{\partial R_{II}} \frac{d\mathbf{k}}{(2\pi)^2}. \tag{33}$$

The solutions of both Eqs. (31) and (33) will be obtained in the next section, following a numerical procedure described in great detail in Appendices B and C.

III. MEAN-FIELD RESULTS

In order to investigate the interplay between both Θ_{II} -loop-current (LC) and QDW orders in the present three-

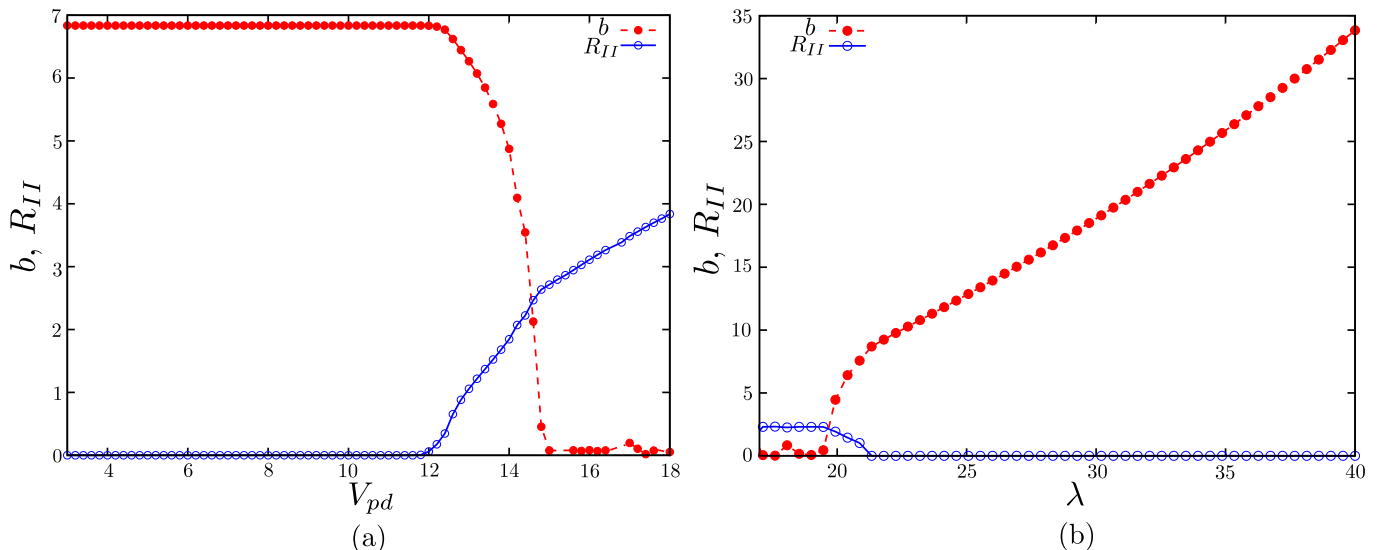


FIG. 4: (Color online) (a) Mean-field values of R_{II} and b as a function of the nearest-neighbor interaction V_{pd} in the limit of zero temperature for $\lambda = 20$. (b) Mean-field values of R_{II} and b as a function of the spin-fermion coupling λ in the limit of zero temperature for $V_{pd} = 14$. Both solutions in (a) and (b) were obtained by performing numerical integration in momentum space of the self-consistency equations given by Eqs. (31) and (33) with a mesh of 320×320 points in the Brillouin zone. Here $m_a = 10^{-2}$, $\gamma = 10^{-5}$ and the other interactions are set to $t_{pd} = 1$, $t_{pp} = 0.5$, $U_p = 3$, and $\varepsilon_d - \varepsilon_p = 3$. The fermionic density on the O orbital is given by $n_p = 0.6$ and the position of the hot spots is such that $\delta = 0.93$.

band model, we solve numerically the mean-field equations for R_{II} and b . The present numerical approach consists in the discretization of the Brillouin zone with a mesh of 320×320 points. We also make the assumption that the order parameter $b(\varepsilon_n, \mathbf{k})$ does not depend crucially on the frequency and momentum. In this way, we will only investigate the ground state properties of the present model, which therefore allows us to evaluate the Matsubara sums that appear in the mean-field equations exactly. We perform this calculation by either varying the spin-fermion coupling λ or the nearest-neighbor interaction V_{pd} between O and Cu orbitals. In addition, we fix all other couplings in the theory. The corresponding results are shown in Figs. 4(a) and (b). For physically realistic parameters in the present model (here we choose, e.g., $m_a = 10^{-2}$, $\gamma = 10^{-5}$, $t_{pd} = 1$, $t_{pp} = 0.5$, $U_p = 3$, and $\varepsilon_d - \varepsilon_p = 3$), we observe in Fig. 4(a) that the order parameter R_{II} grows continuously from zero to positive values as the interaction V_{pd} is increased for λ fixed. It can be very interesting at this point to make a rough estimate of the magnetic moment associated with the loop currents described by R_{II} obtained here at mean-field level. From Fig. 4(a), we can estimate numerically that the ratio of the critical parameters is given approximately by $(R_{II}^c/V_{pd}^c) \sim 0.2$. Hence, by following the same calculation procedure that was explained in detail in Ref.⁴⁸, we may conclude that the Θ_{II} -loop-current phase in our present theory yields a magnetic moment per unit-cell of approximately $M_{LC} \sim 0.19\mu_B$. Quite surprisingly, this result agrees qualitatively with the experimental estimate of $M_{exp} \sim 0.05\mu_B - 0.1\mu_B$ found by Fauqué *et al.*²⁶ using

spin-polarized neutron scattering experiments. In Fig. 4(a), it can also be seen that the QDW order parameter b , by contrast, vanishes as the interaction V_{pd} becomes stronger. Moreover, one can note in the same figure a narrow region where both order parameters can be finite for moderate V_{pd} , indicating that the present three-band model could in principle accommodate a coexisting phase involving both time-reversal (LC order) and translational symmetry breaking (QDW order), but as can be inferred from Fig. 4(a) this apparently occurs for somewhat fine-tuned interactions.

We can also analyze the behavior of the same order parameters as a function of spin-fermion coupling λ , when we keep instead the interaction V_{pd} fixed. The corresponding results are depicted in Fig. 4(b). As a result, we find that the LC order parameter R_{II} is finite below a threshold of λ and then is clearly suppressed when this interaction becomes larger. Once more, the behavior of the QDW order parameter b is essentially the opposite one, namely, it grows from zero to finite values as the spin-fermion interaction becomes stronger. In an analogous way to the previous case, there is also a very narrow window where both phases may coexist for moderate λ and V_{pd} . Despite this, the generic behavior which can be inferred from both figures is that the LC order appears to be detrimental to the QDW order and vice-versa. In other words, we may conclude at this point that, for a large majority of initial choices for the couplings V_{pd} and λ within the present three-band model, there is a strong tendency for the above two orders not to coexist, at least at mean-field level.

In order to analyze the sensitivity of the above mean-field results to changes in the physical parameters of the three-band model, we have also investigated its properties with respect to varying both the spin-wave bosonic mass m_a and the orbital-energy transfer $\varepsilon_d - \varepsilon_p$. As the strength of m_a becomes larger (which corresponds naturally to shorter SDW correlation lengths), we obtain a clear tendency for both critical interactions (i.e. λ_c and V_{pd}^c) to increase even further in our numerical data. This result would of course lie beyond the regime of applicability of a mean-field approach to the present model and other complementary methods that include quantum fluctuation effects should be used to describe such a regime. In addition to this, we have also examined the dependence of our results with respect to changes in the orbital-energy transfer of the model. As a consequence, we were able to establish numerically that, as the difference $\varepsilon_d - \varepsilon_p$ is reduced towards zero, the critical interactions λ_c and V_{pd}^c also display a tendency to increase further within the present approach.

IV. CONCLUSIONS

In the present work, we have performed a consistent mean-field calculation for the three-band (Emery) model relevant to the phenomenology of the underdoped cuprates. We have shown that a low-energy effective description of this model may indeed exhibit both the Θ_{II} -loop-current order first proposed by Varma²⁴ and the so-called QDW which arises from an emergent $SU(2)$ pseudospin symmetry that exists in the spin-fermion model^{15,16}. As a result, we have obtained that the above two order parameters have a tendency to be detrimental to each other, at least at mean-field level.

We would like to point out that the mean-field values of the critical interactions to obtain these two phases are relatively large compared with some physical parameters of the three-band model. This is expected to be an artifact of the mean-field approach and, for this reason, other complementary methods (such as, e.g., renormalization group techniques that include quantum fluctuation effects) should be used in order to establish a quantitative agreement between the present model and the experimental data. It is also important to mention that there are other works in the literature, which analyzed three-band models using weak-coupling diagrammatic perturbative calculations^{49,50}. They have confirmed that the QDW order with a d -wave form factor investigated in the present work turns out to be more stable than the experimentally observed charge order with a modulation along the axial directions. Here, we have shown that the three-band model can also accommodate a Θ_{II} -loop-current phase that breaks time-reversal symmetry, which seemingly acts against the QDW order. This suggests an appealing scenario where the Θ_{II} -loop-current-order strongly competes with the QDW order, with one order having a tendency to suppress the other (and vice-versa)

in the present model. This clearly opens an interesting avenue for future research and may help rule out recent competing (and mutually exclusive) interpretations of the universal phenomenon of the pseudogap phase displayed in the underdoped cuprates, in light of the many highly-precise experiments performed in those materials in the last years.

V. ACKNOWLEDGMENTS

One of us (V. S. de C.) would like to thank a fellowship from CAPES (No. 99999.000324/2014-00) under the program ‘Science Without Borders’. He also acknowledges the kind hospitality of the IPHT in CEA-Saclay during his stay and useful conversations with Salviano Leão. H. F. acknowledges the support from FAPEG under the grant No. 201210267001167. This work was supported partly by LabEx PALM (ANR-10-LABX-0039-PALM), by the ANR project UNESCOS ANR-14-CE05-0007, as well as the grant Ph743-12 of the COFECUB which enabled frequent visits to the International Institute of Physics (IIP), in Natal. X.M. and T.K. also acknowledge the support of CAPES and funding from the IIP.

Appendix A: Definition of the $\hat{\Gamma}_i$ matrices

The matrices $\hat{\Gamma}_1$, $\hat{\Gamma}_2$, $\hat{\Gamma}_{1x}$, $\hat{\Gamma}_{2x}$, $\hat{\Gamma}_{1y}$, and $\hat{\Gamma}_{2y}$ that appear throughout this work are defined by linearizing the functions of the three-band model around the hot spots depicted in Fig. 3. The structure of the resulting matrices can then be simplified by resorting to a representation based on Pauli matrices defined in distinct pseudospin spaces¹⁶, which are denoted by Σ , Λ , and L . Technically speaking, the pseudospin space Σ connects hot spots that can be mapped onto each other by the antiferromagnetic wavevector $\mathbf{Q} = (\pi, \pi)$. Different pairs of hot spots connected by the wavevector \mathbf{Q} are mapped onto each other by the pseudospin space Λ . Lastly, the pseudospin space L connects orthogonal quartet of hot spots. Following these definitions, the matrices of the three-band model can be simply written as

$$\hat{\Gamma}_1 = -2t_{pp} \cos \delta \mathbb{1}_\Sigma \otimes \mathbb{1}_\Lambda \otimes \mathbb{1}_L, \quad (\text{A1})$$

$$\begin{aligned} \hat{\Gamma}_2 &= t_{pp}(\sin \delta \Lambda_3 \otimes L_3 - \Sigma_3 \otimes \Lambda_3) i \partial_x \\ &\quad - t_{pp}(\sin \delta \Lambda_3 + \Sigma_3 \otimes \Lambda_3 \otimes L_3) i \partial_y, \end{aligned} \quad (\text{A2})$$

$$\hat{\Gamma}_{1x} = \gamma_1 e^{-i\varphi \Lambda_3 \otimes L_3} + \gamma_2 e^{i\theta \Lambda_3 \otimes L_3} \Sigma_3 \otimes L_3, \quad (\text{A3})$$

$$\hat{\Gamma}_{2x} = -\frac{1}{2} \gamma_1 e^{-i\varphi \Lambda_3 \otimes L_3} \Sigma_3 \otimes \Lambda_3 + \frac{1}{2} \gamma_2 e^{i\theta \Lambda_3 \otimes L_3} \Lambda_3 \otimes L_3, \quad (\text{A4})$$

$$\hat{\Gamma}_{1y} = \gamma_1 e^{i\varphi \Lambda_3} - \gamma_2 e^{-i\theta \Lambda_3} \Sigma_3 \otimes L_3, \quad (\text{A5})$$

$$\hat{\Gamma}_{2y} = -\frac{1}{2} \gamma_1 e^{i\varphi \Lambda_3} \Sigma_3 \otimes \Lambda_3 \otimes L_3 + \frac{1}{2} \gamma_2 e^{-i\theta \Lambda_3} \Lambda_3, \quad (\text{A6})$$

where $\delta = (K_+ - K_-)/2$ and $\mathbb{1}_\Sigma$, $\mathbb{1}_\Lambda$, and $\mathbb{1}_L$ are, respectively, the identity matrices in the Σ , Λ , and L pseudospin spaces. The parameters φ , θ , γ_1 , and γ_2 are defined as

$$\tan \varphi = \frac{R_{II}}{2t_{pd}} \tan\left(\frac{\delta}{2}\right), \quad (\text{A7})$$

$$\tan \theta = \frac{R_{II}}{2t_{pd}} \cot\left(\frac{\delta}{2}\right), \quad (\text{A8})$$

$$\gamma_1 = \left[2t_{pd}^2 \cos^2\left(\frac{\delta}{2}\right) + \frac{R_{II}^2}{2} \sin^2\left(\frac{\delta}{2}\right) \right]^{1/2}, \quad (\text{A9})$$

$$\gamma_2 = \left[2t_{pd}^2 \sin^2\left(\frac{\delta}{2}\right) + \frac{R_{II}^2}{2} \cos^2\left(\frac{\delta}{2}\right) \right]^{1/2}. \quad (\text{A10})$$

Appendix B: Evaluation of the Matsubara sums for the mean-field equations

1. Quadrupole density wave (QDW) order parameter

In order to compute the Matsubara sum in Eq. (31), we will consider that the QDW order parameter does not depend on both the frequency and the momentum. In this manner, we can rewrite this equation as

$$b(T) = \frac{3\lambda^2 T}{16} \sum_{l,m=1}^2 \sum_{\varepsilon_n} \int \frac{D_{eff}(\varepsilon_n, \mathbf{k})}{\mathcal{D}_l^{(m)}(i\varepsilon_n, \mathbf{k})} \frac{\partial \mathcal{D}_l^{(m)}(i\varepsilon_n, \mathbf{k})}{\partial b} \frac{d\mathbf{k}}{(2\pi)^2}, \quad (\text{B1})$$

where we have not written explicitly the full dependence of $b(T)$ to not clutter up the notation.

There is a subtlety to obtain the analytic continuation of the effective bosonic propagator $D_{eff}(\varepsilon_n, \mathbf{k})$ since this function depends on $|\omega|$ which is not well-defined for complex numbers. To circumvent that, we make use of the two integral formulas

$$|\omega| = -\frac{i\omega}{\pi} \int_{-\infty}^{\infty} \frac{dx}{x - i\omega}, \quad (\text{B2})$$

$$\text{sgn}(\omega) = -\frac{i}{\pi} \int_{-\infty}^{\infty} \frac{dx}{x - i\omega}. \quad (\text{B3})$$

As a result, the analytic continuation of $D_{eff}(\varepsilon_n, \mathbf{k})$ becomes

$$D_{eff}(-iz, \mathbf{k}) = \frac{1}{-i\gamma z \text{sgn}[\text{Im}(z)] + |\mathbf{k}|^2 + m_a}. \quad (\text{B4})$$

As may be easily concluded, $D_{eff}(-iz, \mathbf{k})$ is not analytic in the entire complex plane. Indeed, it possesses a branch cut (see Fig. 5) which must be avoided when performing complex integration. As a result, we obtain that Eq.

(B1) may be rewritten as

$$\begin{aligned} b(T) &= \frac{3\lambda^2}{16} \sum_{l,m=1}^2 \int \frac{d\mathbf{k}}{(2\pi)^2} \left\{ -\frac{1}{2\pi i} \oint_{C_1} dz n_F(z) D_{eff}(-iz, \mathbf{k}) \right. \\ &\times \left. \left[\frac{1}{h_l^{(m)}(z, \mathbf{k})} \frac{\partial h_l^{(m)}(z, \mathbf{k})}{\partial b} + \frac{1}{\bar{h}_l^{(m)}(z, \mathbf{k})} \frac{\partial \bar{h}_l^{(m)}(z, \mathbf{k})}{\partial b} \right] \right\}, \quad (\text{B5}) \end{aligned}$$

where we have used the result $\mathcal{D}_l^{(m)}(z, \mathbf{k}) = h_l^{(m)}(z, \mathbf{k}) \bar{h}_l^{(m)}(z, \mathbf{k})$ (see the Appendix C for details).

Here $h_l^{(m)}(z, \mathbf{k})$ and $\frac{\partial h_l^{(m)}(z, \mathbf{k})}{\partial b}$ are both polynomials with respect to z and the relation between their degrees is the following

$$\deg\left[\frac{\partial h_l^{(m)}(z, \mathbf{k})}{\partial b}\right] < \deg[h_l^{(m)}(z, \mathbf{k})]. \quad (\text{B6})$$

As expected, a similar inequality holds for $\bar{h}_l^{(m)}(z, \mathbf{k})$ and $\frac{\partial \bar{h}_l^{(m)}(z, \mathbf{k})}{\partial b}$. The main consequence of the result in Eq. (B6) is that we can have a series expansion of the form

$$\begin{aligned} &\frac{1}{h_l^{(m)}(z, \mathbf{k})} \frac{\partial h_l^{(m)}(z, \mathbf{k})}{\partial b} + \frac{1}{\bar{h}_l^{(m)}(z, \mathbf{k})} \frac{\partial \bar{h}_l^{(m)}(z, \mathbf{k})}{\partial b} \\ &= \sum_{n=1}^N \frac{\Delta_{l,n}^{(m)}(\mathbf{k})}{z - \xi_{l,n}^{(m)}(\mathbf{k})}, \quad (\text{B7}) \end{aligned}$$

where $N \equiv \frac{3}{4} \dim(\Sigma \otimes \Lambda \otimes L \otimes \tau)$ is equal to twelve and $\xi_{l,n}^{(m)}(\mathbf{k})$ represent both the roots of $h_l^{(m)}(z, \mathbf{k})$ ($1 \leq n \leq N/2$) and $\bar{h}_l^{(m)}(z, \mathbf{k})$ ($N/2 + 1 \leq n \leq N$). The coefficients $\Delta_{l,n}^{(m)}(\mathbf{k})$ are calculated as

$$\begin{aligned} \Delta_{l,n}^{(m)}(\mathbf{k}) &= \frac{\left. \frac{\partial h_l^{(m)}(z, \mathbf{k})}{\partial b} \right|_{z=\xi_{l,n}^{(m)}(\mathbf{k})}}{\left. \frac{\partial h_l^{(m)}(z, \mathbf{k})}{\partial z} \right|_{z=\xi_{l,n}^{(m)}(\mathbf{k})}}, \quad 1 \leq n \leq \frac{N}{2}; \quad (\text{B8}) \\ \Delta_{l,n}^{(m)}(\mathbf{k}) &= \frac{\left. \frac{\partial \bar{h}_l^{(m)}(z, \mathbf{k})}{\partial b} \right|_{z=\xi_{l,n}^{(m)}(\mathbf{k})}}{\left. \frac{\partial \bar{h}_l^{(m)}(z, \mathbf{k})}{\partial z} \right|_{z=\xi_{l,n}^{(m)}(\mathbf{k})}}, \quad \frac{N}{2} + 1 \leq n \leq N. \quad (\text{B9}) \end{aligned}$$

Then by substituting Eq. (B7) into Eq. (B5), we obtain that the mean-field equation for $b(T)$ assumes the

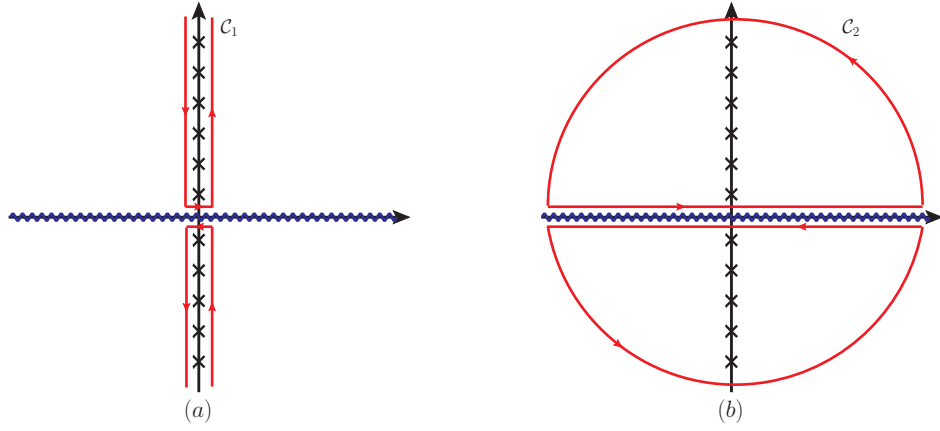


FIG. 5: (a) Integration contour \mathcal{C}_1 for the evaluation of the Matsubara sum appearing in the mean-field equation for the QDW order parameter. The crosses (\times) represent the poles of the Fermi-Dirac distribution function $n_F(z)$ and the wavy-blue line at $\text{Im}(z) = 0$ is the branch cut of $D_{eff}(-iz, \mathbf{k})$. (b) In order to perform the Matsubara sum in this case, the integration contour \mathcal{C}_1 can be distorted such that it transforms into the contour \mathcal{C}_2 that avoids the poles of $n_F(z)$ and also the branch cut.

form

$$b(T) = \frac{3\lambda^2}{16} \sum_{l,m=1}^2 \sum_{n=1}^N \int \Delta_{l,n}^{(m)}(\mathbf{k}) \left[-\frac{1}{2\pi i} \oint_{\mathcal{C}_1} dz n_F(z) \times \frac{D_{eff}(-iz, \mathbf{k})}{z - \xi_{l,n}^{(m)}(\mathbf{k})} \right] \frac{d\mathbf{k}}{(2\pi)^2}. \quad (\text{B10})$$

The complex integral between brackets is computed by changing the integration contour from \mathcal{C}_1 to \mathcal{C}_2 (see Fig. 5), i.e.,

$$\begin{aligned} & -\frac{1}{2\pi i} \oint_{\mathcal{C}_1} dz n_F(z) \frac{D_{eff}(-iz, \mathbf{k})}{z - \xi_{l,n}^{(m)}(\mathbf{k})} \\ &= -\frac{1}{2\pi i} \int_{-\infty}^{\infty} dx n_F(x) \left[\frac{1}{-i\gamma x + |\mathbf{k}|^2 + m_a} \frac{1}{x^+ - \xi_{l,n}^{(m)}(\mathbf{k})} \right. \\ & \quad \left. - \frac{1}{i\gamma x + |\mathbf{k}|^2 + m_a} \frac{1}{x^- - \xi_{l,n}^{(m)}(\mathbf{k})} \right], \quad (\text{B11}) \end{aligned}$$

where $x^\pm = x \pm i\eta$ and $\eta \rightarrow 0^+$. At this point, we employ the Dirac identity

$$\frac{1}{x \pm i\eta} = \mp i\pi\delta(x) + \mathcal{P}\left(\frac{1}{x}\right), \quad (\text{B12})$$

with \mathcal{P} standing for the Cauchy principal value in order to obtain the following

$$\begin{aligned} & -\frac{1}{2\pi i} \oint_{\mathcal{C}_1} dz n_F(z) \frac{D_{eff}(-iz, \mathbf{k})}{z - \xi_{l,n}^{(m)}(\mathbf{k})} \\ &= \frac{|\mathbf{k}|^2 + m_a}{[|\mathbf{k}|^2 + m_a]^2 + \gamma^2[\xi_{l,n}^{(m)}(\mathbf{k})]^2} n_F[\xi_{l,n}^{(m)}(\mathbf{k})] \\ & - \frac{\gamma}{\pi} \mathcal{P} \int_{-\infty}^{\infty} dx \frac{x n_F(x)}{[|\mathbf{k}|^2 + m_a]^2 + \gamma^2 x^2} \frac{1}{x - \xi_{l,n}^{(m)}(\mathbf{k})}. \quad (\text{B13}) \end{aligned}$$

Finally after inserting the result in Eq. (B13) into Eq. (B10), the mean-field equation for the QDW order parameter at finite temperature can be simply expressed as

$$\begin{aligned} b(T) &= \frac{3\lambda^2}{16} \sum_{l,m=1}^2 \sum_{n=1}^N \int \left\{ \frac{|\mathbf{k}|^2 + m_a}{[|\mathbf{k}|^2 + m_a]^2 + \gamma^2[\xi_{l,n}^{(m)}(\mathbf{k})]^2} \right. \\ & \quad \times n_F[\xi_{l,n}^{(m)}(\mathbf{k})] - \frac{\gamma}{\pi} \mathcal{P} \int_{-\infty}^{\infty} dx \frac{x n_F(x)}{[|\mathbf{k}|^2 + m_a]^2 + \gamma^2 x^2} \\ & \quad \left. \times \frac{1}{x - \xi_{l,n}^{(m)}(\mathbf{k})} \right\} \Delta_{l,n}^{(m)}(\mathbf{k}) \frac{d\mathbf{k}}{(2\pi)^2}. \quad (\text{B14}) \end{aligned}$$

In the limit of $T \rightarrow 0$, the Fermi-Dirac distribution function $n_F(x)$ becomes the step function $\theta(-x)$. As a result, the integral in Eq. (B14) involving the Cauchy principal value evaluates to

$$\begin{aligned} & \lim_{T \rightarrow 0} \mathcal{P} \int_{-\infty}^{\infty} dx \frac{x n_F(x)}{[|\mathbf{k}|^2 + m_a]^2 + \gamma^2 x^2} \frac{1}{x - \xi_{l,n}^{(m)}(\mathbf{k})} \\ &= \frac{\pi}{2\gamma} \frac{|\mathbf{k}|^2 + m_a}{[|\mathbf{k}|^2 + m_a]^2 + \gamma^2[\xi_{l,n}^{(m)}(\mathbf{k})]^2} \\ & + \frac{\xi_{l,n}^{(m)}(\mathbf{k})}{([|\mathbf{k}|^2 + m_a]^2 + \gamma^2[\xi_{l,n}^{(m)}(\mathbf{k})]^2)} \ln \left[\frac{\gamma|\xi_{l,n}^{(m)}(\mathbf{k})|}{|\mathbf{k}|^2 + m_a} \right], \quad (\text{B15}) \end{aligned}$$

where now $m_a = m_a(T = 0)$ is the zero-temperature bosonic mass. Hence in this limit the mean-field equation

for the QDW order parameter is given by

$$\begin{aligned}
b(T=0) = & -\frac{3\lambda^2}{32} \sum_{l,m=1}^2 \sum_{n=1}^N \int \left\{ \frac{|\mathbf{k}|^2 + m_a}{(|\mathbf{k}|^2 + m_a)^2 + \gamma^2[\xi_{l,n}^{(m)}(\mathbf{k})]^2} \right. \\
& \times \operatorname{sgn}[\xi_{l,n}^{(m)}(\mathbf{k})] + \frac{2}{\pi} \frac{\gamma \xi_{l,n}^{(m)}(\mathbf{k})}{(|\mathbf{k}|^2 + m_a)^2 + \gamma^2[\xi_{l,n}^{(m)}(\mathbf{k})]^2} \\
& \left. \times \ln \left[\frac{\gamma |\xi_{l,n}^{(m)}(\mathbf{k})|}{|\mathbf{k}|^2 + m_a} \right] \right\} \Delta_{l,n}^{(m)}(\mathbf{k}) \frac{d\mathbf{k}}{(2\pi)^2}, \quad (\text{B16})
\end{aligned}$$

where we have used the identity $\theta(-x) = \frac{1}{2}[1 - \operatorname{sgn}(x)]$ in order to simplify the above equation.

2. Θ_{II} -loop-current (LC) order parameter

The mean-field equation for the loop-current order parameter can be simplified following the same procedure outlined above. First of all, we transform the Matsubara sum in Eq. (33) into an integral over the complex plane. This leads to

$$\begin{aligned}
R_{II}(T) = & \frac{V_{pd}}{2} \sum_{l,m=1}^2 \int \left\{ -\frac{1}{2\pi i} \oint_{\mathcal{C}_1} dz n_F(z) \left[\frac{1}{h_l^{(m)}(z, \mathbf{k})} \right. \right. \\
& \left. \left. \times \frac{\partial h_l^{(m)}(z, \mathbf{k})}{\partial R_{II}} + \frac{1}{\bar{h}_l^{(m)}(z, \mathbf{k})} \frac{\partial \bar{h}_l^{(m)}(z, \mathbf{k})}{\partial R_{II}} \right] \right\} \frac{d\mathbf{k}}{(2\pi)^2}. \quad (\text{B17})
\end{aligned}$$

Then we expand the terms between brackets in the above equation in a series of partial fractions, i.e.,

$$\begin{aligned}
& \frac{1}{h_l^{(m)}(z, \mathbf{k})} \frac{\partial h_l^{(m)}(z, \mathbf{k})}{\partial R_{II}} + \frac{1}{\bar{h}_l^{(m)}(z, \mathbf{k})} \frac{\partial \bar{h}_l^{(m)}(z, \mathbf{k})}{\partial R_{II}} \\
& = \sum_{n=1}^N \frac{\Xi_{l,n}^{(m)}(\mathbf{k})}{z - \xi_{l,n}^{(m)}(\mathbf{k})}, \quad (\text{B18})
\end{aligned}$$

where the coefficients of the expansion $\Xi_{l,n}^{(m)}(\mathbf{k})$ are given by

$$\begin{aligned}
\Xi_{l,n}^{(m)}(\mathbf{k}) = & \frac{\left. \frac{\partial h_l^{(m)}(z, \mathbf{k})}{\partial R_{II}} \right|_{z=\xi_{l,n}^{(m)}(\mathbf{k})}}{\left. \frac{\partial h_l^{(m)}(z, \mathbf{k})}{\partial z} \right|_{z=\xi_{l,n}^{(m)}(\mathbf{k})}}, \quad 1 \leq n \leq \frac{N}{2}; \quad (\text{B19})
\end{aligned}$$

$$\begin{aligned}
\Xi_{l,n}^{(m)}(\mathbf{k}) = & \frac{\left. \frac{\partial \bar{h}_l^{(m)}(z, \mathbf{k})}{\partial R_{II}} \right|_{z=\xi_{l,n}^{(m)}(\mathbf{k})}}{\left. \frac{\partial \bar{h}_l^{(m)}(z, \mathbf{k})}{\partial z} \right|_{z=\xi_{l,n}^{(m)}(\mathbf{k})}}, \quad \frac{N}{2} + 1 \leq n \leq N. \quad (\text{B20})
\end{aligned}$$

Having in mind the result in Eq. (B18), we evaluate the complex integral in Eq. (B17) as

$$\begin{aligned}
& -\frac{1}{2\pi i} \sum_{n=1}^N \Xi_{l,n}^{(m)}(\mathbf{k}) \oint_{\mathcal{C}_1} dz \frac{n_F(z)}{z - \xi_{l,n}^{(m)}(\mathbf{k})} \\
& = \sum_{n=1}^N \Xi_{l,n}^{(m)}(\mathbf{k}) n_F[\xi_{l,n}^{(m)}(\mathbf{k})]. \quad (\text{B21})
\end{aligned}$$

Lastly the mean-field equation for the loop-current order parameter at finite temperature is obtained by inserting Eq. (B21) into Eq. (B17). Therefore this yields

$$R_{II}(T) = \frac{V_{pd}}{2} \sum_{l,m=1}^2 \sum_{n=1}^N \int \Xi_{l,n}^{(m)}(\mathbf{k}) n_F[\xi_{l,n}^{(m)}(\mathbf{k})] \frac{d\mathbf{k}}{(2\pi)^2}. \quad (\text{B22})$$

In the limit of zero temperature, this equation becomes

$$R_{II}(T=0) = \frac{V_{pd}}{2} \sum_{l,m=1}^2 \sum_{n=1}^N \int \Xi_{l,n}^{(m)}(\mathbf{k}) \theta[-\xi_{l,n}^{(m)}(\mathbf{k})] \frac{d\mathbf{k}}{(2\pi)^2}, \quad (\text{B23})$$

with $\theta(-x)$ being the Fermi-Dirac distribution function $n_F(x)$ in this case.

Appendix C: Form of the functions $\mathcal{D}_l^{(m)}(i\varepsilon_n, \mathbf{k})$

In order to compute the determinant $\det[G^{-1}(i\varepsilon_n, \mathbf{k})]$ that appears in the main text of this work, we need to make use of the Eqs. (28) and (29). Then as we are interested in the interplay between loop-current and quadrupole density wave orders, we also neglect the superconducting sector of the matrix \hat{u}_τ . As a result, this determinant evaluates to

$$\det[G^{-1}(i\varepsilon_n, \mathbf{k})] = \prod_{l=1}^2 \prod_{m=1}^2 \mathcal{D}_l^{(m)}(i\varepsilon_n, \mathbf{k}), \quad (\text{C1})$$

where $\mathcal{D}_l^{(m)}(i\varepsilon_n, \mathbf{k})$ are functions whose form will be determined in this appendix.

Before proceeding with that, let us define the following coefficients

$$c_1(k_x) = \sqrt{2} \left(-t_{pd} + i \frac{R_{II}}{4} k_x \right), \quad (\text{C2})$$

$$c_1(k_y) = \sqrt{2} \left(-t_{pd} + i \frac{R_{II}}{4} k_y \right), \quad (\text{C3})$$

$$c_2(k_x) = \frac{\sqrt{2}}{2} (-t_{pd} k_x - i R_{II}), \quad (\text{C4})$$

$$c_2(k_y) = \frac{\sqrt{2}}{2} (-t_{pd} k_y - i R_{II}), \quad (\text{C5})$$

which are written as a function of Cu-O hopping t_{pd} , the loop-current order parameter R_{II} , and the momentum distance \mathbf{k} to the hot spots. The purpose of defining

these four coefficients is of course to write down the functions $\mathcal{D}_l^{(m)}(i\varepsilon_n, \mathbf{k})$ in a compact form.

We then construct the set of basis functions shown in Table I from the hot-spot parameter $\delta = (K_+ - K_-)/2$

and the $c_i(k_x)$, $c_i(k_y)$ ($i = 1, 2$). As a consequence, we can write explicitly the $\mathcal{D}_l^{(m)}(i\varepsilon_n, \mathbf{k})$ as

$$\begin{aligned} \mathcal{D}_1^{(1)}(i\varepsilon_n, \mathbf{k}) &= |\{(-i\varepsilon_n + \xi_d)[(-i\varepsilon_n + \xi_p)^2 - t_{pp}^2(a_1(\mathbf{k}) + b_1(\mathbf{k}))] - P_1^{(0)}(\mathbf{k})(-i\varepsilon_n + \xi_p) - t_{pp}P_1^{(1)}(\mathbf{k})\} \\ &\quad \times \{(-i\varepsilon_n + \xi_d)[(-i\varepsilon_n + \xi_p)^2 - t_{pp}^2(a_2(\mathbf{k}) + b_2(\mathbf{k}))] - P_2^{(0)}(\mathbf{k})(-i\varepsilon_n + \xi_p) - t_{pp}P_2^{(1)}(\mathbf{k})\} \\ &\quad - b^2[(-i\varepsilon_n + \xi_p)^2 - t_{pp}^2(a_1(\mathbf{k}) + b_1(\mathbf{k}))][(-i\varepsilon_n + \xi_p)^2 - t_{pp}^2(a_2(\mathbf{k}) + b_2(\mathbf{k}))]|^2, \end{aligned} \quad (C6)$$

$$\begin{aligned} \mathcal{D}_1^{(2)}(i\varepsilon_n, \mathbf{k}) &= |\{(-i\varepsilon_n + \xi_d)[(-i\varepsilon_n + \xi_p)^2 - t_{pp}^2(a_1(\mathbf{k}) - b_1(\mathbf{k}))] - M_1^{(0)}(\mathbf{k})(-i\varepsilon_n + \xi_p) - t_{pp}M_1^{(1)}(\mathbf{k})\} \\ &\quad \times \{(-i\varepsilon_n + \xi_d)[(-i\varepsilon_n + \xi_p)^2 - t_{pp}^2(a_2(\mathbf{k}) - b_2(\mathbf{k}))] - M_2^{(0)}(\mathbf{k})(-i\varepsilon_n + \xi_p) - t_{pp}M_2^{(1)}(\mathbf{k})\} \\ &\quad - b^2[(-i\varepsilon_n + \xi_p)^2 - t_{pp}^2(a_1(\mathbf{k}) - b_1(\mathbf{k}))][(-i\varepsilon_n + \xi_p)^2 - t_{pp}^2(a_2(\mathbf{k}) - b_2(\mathbf{k}))]|^2, \end{aligned} \quad (C7)$$

$$\begin{aligned} \mathcal{D}_2^{(1)}(i\varepsilon_n, \mathbf{k}) &= |\{(-i\varepsilon_n + \xi_d)[(-i\varepsilon_n + \xi_p)^2 - t_{pp}^2(a_3(\mathbf{k}) + b_3(\mathbf{k}))] - P_3^{(0)}(\mathbf{k})(-i\varepsilon_n + \xi_p) - t_{pp}P_3^{(1)}(\mathbf{k})\} \\ &\quad \times \{(-i\varepsilon_n + \xi_d)[(-i\varepsilon_n + \xi_p)^2 - t_{pp}^2(a_4(\mathbf{k}) + b_4(\mathbf{k}))] - P_4^{(0)}(\mathbf{k})(-i\varepsilon_n + \xi_p) - t_{pp}P_4^{(1)}(\mathbf{k})\} \\ &\quad - b^2[(-i\varepsilon_n + \xi_p)^2 - t_{pp}^2(a_3(\mathbf{k}) + b_3(\mathbf{k}))][(-i\varepsilon_n + \xi_p)^2 - t_{pp}^2(a_4(\mathbf{k}) + b_4(\mathbf{k}))]|^2, \end{aligned} \quad (C8)$$

$$\begin{aligned} \mathcal{D}_2^{(2)}(i\varepsilon_n, \mathbf{k}) &= |\{(-i\varepsilon_n + \xi_d)[(-i\varepsilon_n + \xi_p)^2 - t_{pp}^2(a_3(\mathbf{k}) - b_3(\mathbf{k}))] - M_3^{(0)}(\mathbf{k})(-i\varepsilon_n + \xi_p) - t_{pp}M_3^{(1)}(\mathbf{k})\} \\ &\quad \times \{(-i\varepsilon_n + \xi_d)[(-i\varepsilon_n + \xi_p)^2 - t_{pp}^2(a_4(\mathbf{k}) - b_4(\mathbf{k}))] - M_4^{(0)}(\mathbf{k})(-i\varepsilon_n + \xi_p) - t_{pp}M_4^{(1)}(\mathbf{k})\} \\ &\quad - b^2[(-i\varepsilon_n + \xi_p)^2 - t_{pp}^2(a_3(\mathbf{k}) - b_3(\mathbf{k}))][(-i\varepsilon_n + \xi_p)^2 - t_{pp}^2(a_4(\mathbf{k}) - b_4(\mathbf{k}))]|^2, \end{aligned} \quad (C9)$$

where we have used a second set of basis functions defined in Table II as well as the new functions

$$P_l^{(0)}(\mathbf{k}) = a_{lx}(k_x) + a_{ly}(k_y) + b_{lx}(k_x) + b_{ly}(k_y), \quad (C10)$$

$$P_l^{(1)}(\mathbf{k}) = [\tilde{a}_l(\mathbf{k}) + \tilde{b}_l(\mathbf{k})][a_{lxy}(\mathbf{k}) + b_{lxy}(\mathbf{k})], \quad (C11)$$

$$M_l^{(0)}(\mathbf{k}) = a_{lx}(k_x) + a_{ly}(k_y) - b_{lx}(k_x) - b_{ly}(k_y), \quad (C12)$$

$$M_l^{(1)}(\mathbf{k}) = [\tilde{a}_l(\mathbf{k}) - \tilde{b}_l(\mathbf{k})][a_{lxy}(\mathbf{k}) - b_{lxy}(\mathbf{k})], \quad (C13)$$

which depend on the basis functions of both tables.

In the main text of this paper, we have to perform

the analytic continuation $\varepsilon_n \rightarrow -iz$ for $\mathcal{D}_l^{(m)}(i\varepsilon_n, \mathbf{k})$. By observing the results in Eqs. (C6)–(C9), we conclude that each $\mathcal{D}_l^{(m)}(i\varepsilon_n, \mathbf{k})$ could be written as a product of a function times its complex conjugate. Therefore we can make the analytic continuation as follows

$$\mathcal{D}_l^{(m)}(z, \mathbf{k}) = h_l^{(m)}(z, \mathbf{k})\bar{h}_l^{(m)}(z, \mathbf{k}), \quad (C14)$$

where the functions on the right-hand side of the above equality are given by

$$\begin{aligned} h_1^{(1)}(z, \mathbf{k}) &= \{(z - \xi_d)[(z - \xi_p)^2 - t_{pp}^2(a_1(\mathbf{k}) + b_1(\mathbf{k}))] - P_1^{(0)}(\mathbf{k})(z - \xi_p) + t_{pp}P_1^{(1)}(\mathbf{k})\} \\ &\quad \times \{(z - \xi_d)[(z - \xi_p)^2 - t_{pp}^2(a_2(\mathbf{k}) + b_2(\mathbf{k}))] - P_2^{(0)}(\mathbf{k})(z - \xi_p) + t_{pp}P_2^{(1)}(\mathbf{k})\} \\ &\quad - b^2[(z - \xi_p)^2 - t_{pp}^2(a_1(\mathbf{k}) + b_1(\mathbf{k}))][(z - \xi_p)^2 - t_{pp}^2(a_2(\mathbf{k}) + b_2(\mathbf{k}))], \end{aligned} \quad (C15)$$

$$\begin{aligned} \bar{h}_1^{(1)}(z, \mathbf{k}) &= \{(z + \xi_d)[(z + \xi_p)^2 - t_{pp}^2(a_1(\mathbf{k}) + b_1(\mathbf{k}))] - P_1^{(0)}(\mathbf{k})(z + \xi_p) - t_{pp}P_1^{(1)}(\mathbf{k})\} \\ &\quad \times \{(z + \xi_d)[(z + \xi_p)^2 - t_{pp}^2(a_2(\mathbf{k}) + b_2(\mathbf{k}))] - P_2^{(0)}(\mathbf{k})(z + \xi_p) - t_{pp}P_2^{(1)}(\mathbf{k})\} \\ &\quad - b^2[(z + \xi_p)^2 - t_{pp}^2(a_1(\mathbf{k}) + b_1(\mathbf{k}))][(z + \xi_p)^2 - t_{pp}^2(a_2(\mathbf{k}) + b_2(\mathbf{k}))], \end{aligned} \quad (C16)$$

$$\begin{aligned} h_1^{(2)}(z, \mathbf{k}) &= \{(z - \xi_d)[(z - \xi_p)^2 - t_{pp}^2(a_1(\mathbf{k}) - b_1(\mathbf{k}))] - M_1^{(0)}(\mathbf{k})(z - \xi_p) + t_{pp}M_1^{(1)}(\mathbf{k})\} \\ &\quad \times \{(z - \xi_d)[(z - \xi_p)^2 - t_{pp}^2(a_2(\mathbf{k}) - b_2(\mathbf{k}))] - M_2^{(0)}(\mathbf{k})(z - \xi_p) + t_{pp}M_2^{(1)}(\mathbf{k})\} \\ &\quad - b^2[(z - \xi_p)^2 - t_{pp}^2(a_1(\mathbf{k}) - b_1(\mathbf{k}))][(z - \xi_p)^2 - t_{pp}^2(a_2(\mathbf{k}) - b_2(\mathbf{k}))], \end{aligned} \quad (C17)$$

TABLE I: First set of basis functions used to represent the free energy of the three-band model. Here these functions are written in terms of the hot-spot parameter $\delta = (K_+ - K_-)/2$ and the coefficients $c_i(k_x)$ and $c_i(k_y)$ ($i = 1, 2$).

Basis function	Definition
$a_{1x}(k_x)$	$ c_1(k_x) ^2 + c_2(k_x) ^2$
$a_{2x}(k_x)$	$ c_1(k_x) ^2 + c_2(k_x) ^2$
$a_{3x}(k_x)$	$ c_1(k_x) ^2 + c_2(k_x) ^2$
$a_{4x}(k_x)$	$ c_1(k_x) ^2 + c_2(k_x) ^2$
$b_{1x}(k_x)$	$\sin \delta [c_1(k_x) ^2 - c_2(k_x) ^2] + 2 \cos \delta \operatorname{Re}[c_1^*(k_x)c_2(k_x)]$
$b_{2x}(k_x)$	$\sin \delta [c_1(k_x) ^2 - c_2(k_x) ^2] - 2 \cos \delta \operatorname{Re}[c_1^*(k_x)c_2(k_x)]$
$b_{3x}(k_x)$	$\sin \delta [c_2(k_x) ^2 - c_1(k_x) ^2] + 2 \cos \delta \operatorname{Re}[c_1^*(k_x)c_2(k_x)]$
$b_{4x}(k_x)$	$\sin \delta [c_2(k_x) ^2 - c_1(k_x) ^2] - 2 \cos \delta \operatorname{Re}[c_1^*(k_x)c_2(k_x)]$
$a_{1y}(k_y)$	$ c_1(k_y) ^2 + c_2(k_y) ^2$
$a_{2y}(k_y)$	$ c_1(k_y) ^2 + c_2(k_y) ^2$
$a_{3y}(k_y)$	$ c_1(k_y) ^2 + c_2(k_y) ^2$
$a_{4y}(k_y)$	$ c_1(k_y) ^2 + c_2(k_y) ^2$
$b_{1y}(k_y)$	$\sin \delta [c_2(k_y) ^2 - c_1(k_y) ^2] + 2 \cos \delta \operatorname{Re}[c_1^*(k_y)c_2(k_y)]$
$b_{2y}(k_y)$	$\sin \delta [c_2(k_y) ^2 - c_1(k_y) ^2] - 2 \cos \delta \operatorname{Re}[c_1^*(k_y)c_2(k_y)]$
$b_{3y}(k_y)$	$\sin \delta [c_1(k_y) ^2 - c_2(k_y) ^2] - 2 \cos \delta \operatorname{Re}[c_1^*(k_y)c_2(k_y)]$
$b_{4y}(k_y)$	$\sin \delta [c_1(k_y) ^2 - c_2(k_y) ^2] + 2 \cos \delta \operatorname{Re}[c_1^*(k_y)c_2(k_y)]$
$a_{1xy}(\mathbf{k})$	$2 \cos \delta \operatorname{Re}[c_1^*(k_x)c_1(k_y) + c_2^*(k_x)c_2(k_y)] + 2 \sin \delta \operatorname{Re}[c_1^*(k_x)c_2(k_y) - c_2^*(k_x)c_1(k_y)]$
$a_{2xy}(\mathbf{k})$	$2 \cos \delta \operatorname{Re}[c_1^*(k_x)c_1(k_y) + c_2^*(k_x)c_2(k_y)] - 2 \sin \delta \operatorname{Re}[c_1^*(k_x)c_2(k_y) - c_2^*(k_x)c_1(k_y)]$
$a_{3xy}(\mathbf{k})$	$2 \cos \delta \operatorname{Re}[c_1^*(k_x)c_1(k_y) - c_2^*(k_x)c_2(k_y)] + 2 \sin \delta \operatorname{Re}[c_1^*(k_x)c_2(k_y) + c_2^*(k_x)c_1(k_y)]$
$a_{4xy}(\mathbf{k})$	$2 \cos \delta \operatorname{Re}[c_1^*(k_x)c_1(k_y) - c_2^*(k_x)c_2(k_y)] - 2 \sin \delta \operatorname{Re}[c_1^*(k_x)c_2(k_y) + c_2^*(k_x)c_1(k_y)]$
$b_{1xy}(\mathbf{k})$	$2 \operatorname{Re}[c_2^*(k_x)c_1(k_y) + c_1^*(k_x)c_2(k_y)]$
$b_{2xy}(\mathbf{k})$	$-2 \operatorname{Re}[c_2^*(k_x)c_1(k_y) + c_1^*(k_x)c_2(k_y)]$
$b_{3xy}(\mathbf{k})$	$2 \operatorname{Re}[c_2^*(k_x)c_1(k_y) - c_1^*(k_x)c_2(k_y)]$
$b_{4xy}(\mathbf{k})$	$-2 \operatorname{Re}[c_2^*(k_x)c_1(k_y) - c_1^*(k_x)c_2(k_y)]$

TABLE II: Second set of basis functions needed to evaluate the free energy of the present three-band model. In our notation, the indices l and \tilde{l} refer respectively to the functions $a_l(\mathbf{k})$ [and $b_l(\mathbf{k})$] and $\tilde{a}_l(\mathbf{k})$ [and $\tilde{b}_l(\mathbf{k})$].

l	$a_l(\mathbf{k})$	$b_l(\mathbf{k})$
1	$(k_x + k_y)^2 + \sin^2 \delta (k_y - k_x + 2 \cot \delta)^2$	$2 \sin \delta [(k_y + \cot \delta)^2 - (k_x - \cot \delta)^2]$
2	$(k_x + k_y)^2 + \sin^2 \delta (k_y - k_x - 2 \cot \delta)^2$	$2 \sin \delta [(k_y - \cot \delta)^2 - (k_x + \cot \delta)^2]$
3	$(k_x - k_y)^2 + \sin^2 \delta (k_x + k_y + 2 \cot \delta)^2$	$2 \sin \delta [(k_x + \cot \delta)^2 - (k_y + \cot \delta)^2]$
4	$(k_x - k_y)^2 + \sin^2 \delta (k_x + k_y - 2 \cot \delta)^2$	$2 \sin \delta [(k_x - \cot \delta)^2 - (k_y - \cot \delta)^2]$
$\tilde{1}$	$-\sin \delta (k_x - k_y - 2 \cot \delta)$	$k_x + k_y$
$\tilde{2}$	$\sin \delta (k_x - k_y + 2 \cot \delta)$	$-(k_x + k_y)$
$\tilde{3}$	$\sin \delta (k_x + k_y + 2 \cot \delta)$	$k_x - k_y$
$\tilde{4}$	$-\sin \delta (k_x + k_y - 2 \cot \delta)$	$-(k_x - k_y)$

$$\begin{aligned} \bar{h}_1^{(2)}(z, \mathbf{k}) &= \{(z + \xi_d)[(z + \xi_p)^2 - t_{pp}^2(a_1(\mathbf{k}) - b_1(\mathbf{k}))] - M_1^{(0)}(\mathbf{k})(z + \xi_p) - t_{pp}M_1^{(1)}(\mathbf{k})\} \\ &\quad \times \{(z + \xi_d)[(z + \xi_p)^2 - t_{pp}^2(a_2(\mathbf{k}) - b_2(\mathbf{k}))] - M_2^{(0)}(\mathbf{k})(z + \xi_p) - t_{pp}M_2^{(1)}(\mathbf{k})\} \\ &\quad - b^2[(z + \xi_p)^2 - t_{pp}^2(a_1(\mathbf{k}) - b_1(\mathbf{k}))][(z + \xi_p)^2 - t_{pp}^2(a_2(\mathbf{k}) - b_2(\mathbf{k}))], \end{aligned} \quad (\text{C18})$$

$$\begin{aligned} h_2^{(1)}(z, \mathbf{k}) &= \{(z - \xi_d)[(z - \xi_p)^2 - t_{pp}^2(a_3(\mathbf{k}) + b_3(\mathbf{k}))] - P_3^{(0)}(\mathbf{k})(z - \xi_p) + t_{pp}P_3^{(1)}(\mathbf{k})\} \\ &\quad \times \{(z - \xi_d)[(z - \xi_p)^2 - t_{pp}^2(a_4(\mathbf{k}) + b_4(\mathbf{k}))] - P_4^{(0)}(\mathbf{k})(z - \xi_p) + t_{pp}P_4^{(1)}(\mathbf{k})\} \\ &\quad - b^2[(z - \xi_p)^2 - t_{pp}^2(a_3(\mathbf{k}) + b_3(\mathbf{k}))][(z - \xi_p)^2 - t_{pp}^2(a_4(\mathbf{k}) + b_4(\mathbf{k}))], \end{aligned} \quad (\text{C19})$$

$$\begin{aligned} \bar{h}_2^{(1)}(z, \mathbf{k}) &= \{(z + \xi_d)[(z + \xi_p)^2 - t_{pp}^2(a_3(\mathbf{k}) + b_3(\mathbf{k}))] - P_3^{(0)}(\mathbf{k})(z + \xi_p) - t_{pp}P_3^{(1)}(\mathbf{k})\} \\ &\quad \times \{(z + \xi_d)[(z + \xi_p)^2 - t_{pp}^2(a_4(\mathbf{k}) + b_4(\mathbf{k}))] - P_4^{(0)}(\mathbf{k})(z + \xi_p) - t_{pp}P_4^{(1)}(\mathbf{k})\} \\ &\quad - b^2[(z + \xi_p)^2 - t_{pp}^2(a_3(\mathbf{k}) + b_3(\mathbf{k}))][(z + \xi_p)^2 - t_{pp}^2(a_4(\mathbf{k}) + b_4(\mathbf{k}))], \end{aligned} \quad (\text{C20})$$

$$\begin{aligned}
h_2^{(2)}(z, \mathbf{k}) &= \{(z - \xi_d)[(z - \xi_p)^2 - t_{pp}^2(a_3(\mathbf{k}) - b_3(\mathbf{k}))] - M_3^{(0)}(\mathbf{k})(z - \xi_p) + t_{pp}M_3^{(1)}(\mathbf{k})\} \\
&\times \{(z - \xi_d)[(z + \xi_p)^2 - t_{pp}^2(a_4(\mathbf{k}) - b_4(\mathbf{k}))] - M_4^{(0)}(\mathbf{k})(z - \xi_p) + t_{pp}M_4^{(1)}(\mathbf{k})\} \\
&- b^2[(z - \xi_p)^2 - t_{pp}^2(a_3(\mathbf{k}) - b_3(\mathbf{k}))][(z - \xi_p)^2 - t_{pp}^2(a_4(\mathbf{k}) - b_4(\mathbf{k}))], \tag{C21}
\end{aligned}$$

$$\begin{aligned}
\bar{h}_2^{(2)}(z, \mathbf{k}) &= \{(z + \xi_d)[(z + \xi_p)^2 - t_{pp}^2(a_3(\mathbf{k}) - b_3(\mathbf{k}))] - M_3^{(0)}(\mathbf{k})(z + \xi_p) - t_{pp}M_3^{(1)}(\mathbf{k})\} \\
&\times \{(z + \xi_d)[(z + \xi_p)^2 - t_{pp}^2(a_4(\mathbf{k}) - b_4(\mathbf{k}))] - M_4^{(0)}(\mathbf{k})(z + \xi_p) - t_{pp}M_4^{(1)}(\mathbf{k})\} \\
&- b^2[(z + \xi_p)^2 - t_{pp}^2(a_3(\mathbf{k}) - b_3(\mathbf{k}))][(z + \xi_p)^2 - t_{pp}^2(a_4(\mathbf{k}) - b_4(\mathbf{k}))]. \tag{C22}
\end{aligned}$$

According to the approach developed in the Appendix B for solving the LC and QDW mean-field equations, we need to determine first the roots of $h_l^{(m)}(z, \mathbf{k})$ and $\bar{h}_l^{(m)}(z, \mathbf{k})$ which are denoted here as $\xi_{l,n}^{(m)}(\mathbf{k})$ ($n =$

$1, \dots, N$). As $h_l^{(m)}(z, \mathbf{k})$ and $\bar{h}_l^{(m)}(z, \mathbf{k})$ are both sixth-order polynomials in the variable z , their roots will be determined by means of numerical methods.

* Electronic address: hermann_freire@ufg.br

- ¹ T. Wu, H. Mayaffre, S. Krämer, M. Horvatic, C. Berthier, W. N. Hardy, R. Liang, D. A. Bonn, and M.-H. Julien, *Nature* **477**, 191 (2011).
- ² T. Wu, H. Mayaffre, S. Krämer, M. Horvatic, C. Berthier, P. L. Kuhns, A. P. Reyes, R. Liang, W. N. Hardy, D. A. Bonn, and M.-H. Julien, *Nat. Commun.* **4**, 2113 (2013).
- ³ D. LeBoeuf, S. Krämer, W. N. Hardy, R. Liang, D. A. Bonn, and Cyril Proust, *Nature Physics* **9**, 79 (2013).
- ⁴ G. Ghiringhelli, M. Le Tacon, M. Minola, S. Blanco-Canosa, C. Mazzoli, N. B. Brookes, G. M. De Luca, A. Frano, D. G. Hawthorn, F. He, T. Loew, M. Moretti Sala, D. C. Peets, M. Salluzzo, E. Schierle, R. Sutarto, G. A. Sawatzky, E. Weschke, B. Keimer, and L. Braicovich, *Science* **337**, 821 (2012).
- ⁵ A. J. Achkar, R. Sutarto, X. Mao, F. He, A. Frano, S. Blanco-Canosa, M. Le Tacon, G. Ghiringhelli, L. Braicovich, M. Minola, M. Moretti Sala, C. Mazzoli, R. Liang, D. A. Bonn, W. N. Hardy, B. Keimer, G. A. Sawatzky, and D. G. Hawthorn, *Phys. Rev. Lett.* **109**, 167001 (2012).
- ⁶ J. Chang, E. Blackburn, A. T. Holmes, N. B. Christensen, J. Larsen, J. Mesot, R. Liang, D. A. Bonn, W. N. Hardy, A. Watenphul, M. v. Zimmermann, E. M. Forgan, and S. M. Hayden, *Nat. Phys.* **8**, 871 (2012).
- ⁷ J. E. Hoffman, E. W. Hudson, K. M. Lang, V. Madhavan, H. Eisaki, S. Uchida, and J. C. Davis, *Science* **295**, 466 (2002).
- ⁸ M. Vershinin, S. Misra, S. Ono, Y. Abe, Y. Ando, and A. Yazdani, *Science* **303**, 1995 (2004).
- ⁹ R. Comin, R. Sutarto, F. He, E. da Silva Neto, L. Chauviere, A. Frano, R. Liang, W. N. Hardy, D. Bonn, Y. Yoshida, H. Eisaki, J. E. Hoffman, B. Keimer, G. A. Sawatzky, and A. Damascelli, *Nature Materials* **14**, 796 (2015).
- ¹⁰ K. Fujita, M. H. Hamidian, S. D. Edkins, C. K. Kim, Y. Kohsaka, M. Azuma, M. Takano, H. Takagi, H. Eisaki, S.-i. Uchida, A. Allais, M. J. Lawler, E.-A. Kim, S. Sachdev, and J. C. S. Davis, *Proc. Natl. Acad. Sci.* **111**, E3026 (2014).
- ¹¹ R. Comin, A. Frano, M. M. Yee, Y. Yoshida, H. Eisaki, E. Schierle, E. Weschke, R. Sutarto, F. He, A. Soumya-narayanan, Y. He, M. Le Tacon, I. S. Elfimov, J. E. Hoffman, G. A. Sawatzky, B. Keimer, and A. Damascelli, *Science* **343**, 390 (2014).
- ¹² E. H. da Silva Neto, P. Aynajian, A. Frano, R. Comin, E. Schierle, E. Weschke, A. Gyenis, J. Wen, J. Schneeloch, Z. Xu, S. Ono, G. Gu, M. Le Tacon, and A. Yazdani, *Science* **343**, 393 (2014).
- ¹³ O. Cyr-Choinière, D. LeBoeuf, S. Badoux, S. Dufour-Beauséjour, D. A. Bonn, W. N. Hardy, R. Liang, N. Doiron-Leyraud, and Louis Taillefer, arXiv:1503.02033 (2015).
- ¹⁴ A. Abanov and A. V. Chubukov, *Phys. Rev. Lett.* **84**, 5608 (2000); Ar. Abanov, A. V. Chubukov, and J. Schmalian, *Adv. Phys.* **52**, 119 (2003).
- ¹⁵ M. A. Metlitski and S. Sachdev, *Phys. Rev. B* **82**, 075128 (2010).
- ¹⁶ K. B. Efetov, H. Meier, and C. Pépin, *Nature Physics* **9**, 442 (2013).
- ¹⁷ S. Sachdev and R. La Placa, *Phys. Rev. Lett.* **111**, 027202 (2013).
- ¹⁸ S. E. Sebastian, N. Harrison, and G. G. Lonzarich, *Reports on Progress in Physics* **75**, 102501 (2012).
- ¹⁹ N. Doiron-Leyraud, C. Proust, D. LeBoeuf, J. Levallois, J.-B. Bonnemaison, R. Liang, D. A. Bonn, W. N. Hardy, and L. Taillefer, *Nature* **447**, 565 (2007).
- ²⁰ Y. Li, V. Baledent, N. Barisic, Y. Cho, B. Fauque, Y. Sidis, G. Yu, X. Zhao, P. Bourges, and M. Greven, *Nature* **455**, 372 (2008).
- ²¹ L. Mangin-Thro, Y. Sidis, A. Wildes, and P. Bourges, arXiv:1501.04919.
- ²² J. Xia, E. Schemm, G. Deutscher, S. A. Kivelson, D. A. Bonn, W. N. Hardy, R. Liang, W. Siemons, G. Koster, M. M. Fejer, and A. Kapitulnik, *Phys. Rev. Lett.* **100**, 127002 (2008).
- ²³ H. Karapetyan, J. Xia, M. Hucker, G. D. Gu, J. M. Tranquada, M. M. Fejer, and A. Kapitulnik, *Phys. Rev. Lett.* **112**, 047003 (2014).
- ²⁴ C. M. Varma, *Phys. Rev. B* **73**, 155113 (2006).
- ²⁵ S. Bulut, A. P. Kampf, and W. A. Atkinson, arXiv:1503.08896.
- ²⁶ B. Fauque, Y. Sidis, V. Hinkov, S. Pailhes, C. T. Lin, X. Chaud, and P. Bourges, *Phys. Rev. Lett.* **96**, 197001

- (2006).
- ²⁷ B. J. Ramshaw, S. E. Sebastian, R. D. McDonald, James Day, B. S. Tan, Z. Zhu, J. B. Betts, Ruixing Liang, D. A. Bonn, W. N. Hardy, and N. Harrison, *Science* **348**, 317 (2015).
- ²⁸ H. Meier, C. Pepin, M. Einenkel, and K. B. Efetov, *Phys. Rev. B* **89**, 195115 (2014).
- ²⁹ M. Einenkel, H. Meier, C. Pepin, and K. B. Efetov, *Phys. Rev. B* **90**, 054511 (2014).
- ³⁰ D. Chowdhury and S. Sachdev, *Phys. Rev. B* **90**, 134516 (2014).
- ³¹ J. D. Sau and S. Sachdev, *Phys. Rev. B* **89**, 075129 (2014).
- ³² Y. Wang and A. Chubukov, *Phys. Rev. B* **90**, 035149 (2014).
- ³³ A. Allais, J. Bauer and S. Sachdev, *Phys. Rev. B* **90**, 155114 (2014).
- ³⁴ A. Allais, J. Bauer and S. Sachdev, *Indian Journal of Physics* **88**, 905 (2014).
- ³⁵ A. M. Tsvelik and A. V. Chubukov, *Phys. Rev. B* **89**, 184515 (2014).
- ³⁶ V. S. de Carvalho and H. Freire, *Annals of Physics* **348**, 32 (2014).
- ³⁷ V. S. de Carvalho and H. Freire, *Nuclear Physics B* **875**, 738 (2013).
- ³⁸ P. A. Lee, *Phys. Rev. X* **4**, 031017 (2014).
- ³⁹ D. F. Agterberg, D. S. Melchert, and M. K. Kashyap, *Phys. Rev. B* **91**, 054502 (2015).
- ⁴⁰ E. Fradkin, S. A. Kivelson, and J. M. Tranquada, *Reviews of Modern Physics* **87**, 457 (2015).
- ⁴¹ C. Pepin, V. S. de Carvalho, T. Kloss, and X. Montiel, *Phys. Rev. B* **90**, 195207 (2014); T. Kloss, X. Montiel, and C. Pepin, *Phys. Rev. B* **91**, 205124 (2015).
- ⁴² Y. Wang, D. F. Agterberg, and A. Chubukov, *Phys. Rev. B* **91**, 115103 (2015).
- ⁴³ H. Freire, V. S. de Carvalho, and C. Pepin, *Phys. Rev. B* **92**, 045132 (2015).
- ⁴⁴ V. J. Emery, *Phys. Rev. Lett.* **58**, 2794 (1987).
- ⁴⁵ C. M. Varma, S. Schmitt-Rink, and E. Abrahams, *Solid State Commun.* **62**, 681 (1987).
- ⁴⁶ W. Hanke, M.L. Kiesel, M. Aichhorn, S. Brehm, and E. Arrighi, *European Physical Journal Special Topics* **188**, 15 (2010).
- ⁴⁷ M. H. Fischer and E.-A. Kim, *Phys. Rev. B* **84**, 144502 (2011).
- ⁴⁸ R. Thomale and M. Greiter, *Phys. Rev. B* **77**, 094511 (2008).
- ⁴⁹ S. Bulut, W. A. Atkinson, and A. P. Kampf, *Phys. Rev. B* **88**, 155132 (2013).
- ⁵⁰ A. Thomson and S. Sachdev, *Phys. Rev. B* **91**, 115142 (2015).